The Astrophysical Journal Letters, 973:L14 (20pp), 2024 September 20 https://doi.org/10.3847/2041-8213/ad6f9f

The Dark Energy Survey: Cosmology Results with ∼1500 New High-redshift Type Ia Supernovae Using the Full 5 yr Data Set

DES Collaboration: T. M. C. Abbott[1], M. Acevedo[2], M. Aguena[3], A. Alarcon[4], S. Allam[5], O. Alves[6], A. Amon[7], F. Andrade-Oliveira[6], J. Annis[5], P. Armstrong[8], J. Asorey[9], S. Avila[10], D. Bacon[11], B. A. Bassett[12,13], K. Bechtol[14], P. H. Bernardinelli[15], G. M. Bernstein[16], E. Bertin[17,18], J. Blazek[19], S. Bocquet[20], D. Brooks[21], D. Brout[22], E. Buckley-Geer[5,23], D. L. Burke[24,25], H. Camacho[3,26], R. Camilleri[27], A. Campos[28], A. Carnero Rosell[3,29,30], D. Carollo[31], A. Carr[27], J. Carretero[10], F. J. Castander[32,33], R. Cawthon[34], C. Chang[23,35], R. Chen[2], A. Choi[36], C. Conselice[37,38], M. Costanzi[31,39,40], L. N. da Costa[3], M. Crocce[32,33], T. M. Davis[27], D. L. DePoy[41], S. Desai[42], H. T. Diehl[5], M. Dixon[43], S. Dodelson[28,44], P. Doel[21], C. Doux[16,45], A. Drlica-Wagner[5,23,35], J. Elvin-Poole[46], S. Everett[47], I. Ferrero[48], A. Ferté[25], B. Flaugher[5], R. J. Foley[49], P. Fosalba[32,33], D. Friedel[50], J. Frieman[5,35], C. Frohmaier[51], L. Galbany[32,33], J. García-Bellido[52], M. Gatti[16], E. Gaztanaga[11,32,33], G. Giannini[10,35], K. Glazebrook[43], O. Graur[11], D. Gruen[20], R. A. Gruendl[50,53], G. Gutierrez[5], W. G. Hartley[54], K. Herner[5], S. R. Hinton[27], D. L. Hollowood[55], K. Honscheid[56,57], D. Huterer[6], B. Jain[16], D. J. James[58,59], N. Jeffrey[21], E. Kasai[12,60], L. Kelsey[11], S. Kent[5,35], R. Kessler[23,35], A. G. Kim[61], R. P. Kirshner[62,63], E. Kovacs[4], K. Kuehn[64,65], O. Lahav[21], J. Lee[16], S. Lee[47], G. F. Lewis[66], T. S. Li[67], C. Lidman[8,68], H. Lin[5], U. Malik[8], J. L. Marshall[41], P. Martini[56,69], J. Mena-Fernández[70], F. Menanteau[50,53], R. Miquel[10,71], J. J. Mohr[20,72], J. Mould[43], J. Muir[73], A. Möller[43], E. Neilsen[5], R. C. Nichol[74], P. Nugent[61], R. L. C. Ogando[75], A. Palmese[28], Y.-C. Pan[76], M. Paterno[5], W. J. Percival[46,73], M. E. S. Pereira[77], A. Pieres[3,75], A. A. Plazas Malagón[24,25], B. Popovic[2], A. Porredon[78], J. Prat[35], H. Qu[16], M. Raveri[79], M. Rodríguez-Monroy[80], A. K. Romer[81], A. Roodman[24,25], B. Rose[2,82], M. Sako[16], E. Sanchez[83], D. Sanchez Cid[83], M. Schubnell[6], D. Scolnic[2], I. Sevilla-Noarbe[83], P. Shah[21], J. Allyn. Smith[84], M. Smith[85], M. Soares-Santos[86], E. Suchyta[87], M. Sullivan[51], N. Suntzeff[41], M. E. C. Swanson[50], B. O. Sánchez[88], G. Tarle[6], G. Taylor[8], D. Thomas[11], C. To[56], M. Toy[51], M. A. Troxel[2], B. E. Tucker[8], D. L. Tucker[5], S. A. Uddin[89], M. Vincenzi[2], A. R. Walker[1], N. Weaverdyck[6,61], R. H. Wechsler[24,25,90], J. Weller[72,91], W. Wester[5], P. Wiseman[51], M. Yamamoto[2], F. Yuan[8], B. Zhang[8], and Y. Zhang[1]

[1] Cerro Tololo Inter-American Observatory, NSF's National Optical-Infrared Astronomy Research Laboratory, Casilla 603, La Serena, Chile
[2] Department of Physics, Duke University, Durham, NC 27708, USA
[3] Laboratório Interinstitucional de e-Astronomia—LIneA, Rua Gal. José Cristino 77, Rio de Janeiro, RJ–20921-400, Brazil
[4] Argonne National Laboratory, 9700 South Cass Avenue, Lemont, IL 60439, USA
[5] Fermi National Accelerator Laboratory, P.O. Box 500, Batavia, IL 60510, USA
[6] Department of Physics, University of Michigan, Ann Arbor, MI 48109, USA
[7] Department of Astrophysical Sciences, Princeton University, Princeton, NJ 08544, USA
[8] The Research School of Astronomy and Astrophysics, Australian National University, ACT 2601, Australia
[9] Departamento de Física Teórica and IPARCOS, Universidad Complutense de Madrid, 28040 Madrid, Spain
[10] Institut de Física d'Altes Energies (IFAE), The Barcelona Institute of Science and Technology, Campus UAB, 08193 Bellaterra (Barcelona), Spain
[11] Institute of Cosmology and Gravitation, University of Portsmouth, Portsmouth, PO1 3FX, UK
[12] South African Astronomical Observatory, P.O. Box 9, Observatory 7935, South Africa
[13] Mathematics Department, University of Cape Town, South Africa
[14] Physics Department, 2320 Chamberlin Hall, University of Wisconsin–Madison, 1150 University Avenue, Madison, WI 53706-1390, USA
[15] Astronomy Department, University of Washington, Box 351580, Seattle, WA 98195, USA
[16] Department of Physics and Astronomy, University of Pennsylvania, Philadelphia, PA 19104, USA
[17] CNRS, UMR 7095, Institut d'Astrophysique de Paris, F-75014, Paris, France
[18] Sorbonne Universités, UPMC Univ Paris 06, UMR 7095, Institut d'Astrophysique de Paris, F-75014, Paris, France
[19] Department of Physics, Northeastern University, Boston, MA 02115, USA
[20] University Observatory, Faculty of Physics, Ludwig-Maximilians-Universität, Scheinerstr. 1, 81679 Munich, Germany
[21] Department of Physics & Astronomy, University College London, Gower Street, London, WC1E 6BT, UK
[22] Department of Astronomy and Department of Physics, Boston University, Boston, MA 02140, USA
[23] Department of Astronomy and Astrophysics, University of Chicago, Chicago, IL 60637, USA
[24] Kavli Institute for Particle Astrophysics & Cosmology, P.O. Box 2450, Stanford University, Stanford, CA 94305, USA
[25] SLAC National Accelerator Laboratory, Menlo Park, CA 94025, USA
[26] Instituto de Física Teórica, Universidade Estadual Paulista, São Paulo, Brazil
[27] School of Mathematics and Physics, University of Queensland, Brisbane, QLD 4072, Australia
[28] Department of Physics, Carnegie Mellon University, Pittsburgh, PA 15312, USA
[29] Instituto de Astrofisica de Canarias, E-38205 La Laguna, Tenerife, Spain
[30] Universidad de La Laguna, Dpto. Astrofísica, E-38206 La Laguna, Tenerife, Spain
[31] INAF-Osservatorio Astronomico di Trieste, via G. B. Tiepolo 11, I-34143 Trieste, Italy
[32] Institut d'Estudis Espacials de Catalunya (IEEC), 08034 Barcelona, Spain
[33] Institute of Space Sciences (ICE, CSIC), Campus UAB, Carrer de Can Magrans, s/n, 08193 Barcelona, Spain
[34] Physics Department, William Jewell College, Liberty, MO 64068, USA
[35] Kavli Institute for Cosmological Physics, University of Chicago, Chicago, IL 60637, USA
[36] NASA Goddard Space Flight Center, 8800 Greenbelt Road, Greenbelt, MD 20771, USA
[37] Jodrell Bank Center for Astrophysics, School of Physics & Astronomy, University of Manchester, Oxford Road, Manchester, M139PL, UK
[38] University of Nottingham, School of Physics and Astronomy, Nottingham NG7 2RD, UK
[39] Astronomy Unit, Department of Physics, University of Trieste, via Tiepolo 11, I-34131 Trieste, Italy
[40] Institute for Fundamental Physics of the Universe, Via Beirut 2, 34014 Trieste, Italy
[41] George P. and Cynthia Woods Mitchell Institute for Fundamental Physics and Astronomy and Department of Physics and Astronomy, Texas A&M University, College Station, TX 77843, USA

[42] Department of Physics, IIT Hyderabad, Kandi, Telangana 502285, India
[43] Centre for Astrophysics & Supercomputing, Swinburne University of Technology, VIC 3122, Australia
[44] NSF AI Planning Institute for Physics of the Future, Carnegie Mellon University, Pittsburgh, PA 15213, USA
[45] Université Grenoble Alpes, CNRS, LPSC-IN2P3, 38000 Grenoble, France
[46] Department of Physics and Astronomy, University of Waterloo, 200 University Avenue West, Waterloo, ON N2L 3G1, Canada
[47] Jet Propulsion Laboratory, California Institute of Technology, 4800 Oak Grove Drive, Pasadena, CA 91109, USA
[48] Institute of Theoretical Astrophysics, University of Oslo, P.O. Box 1029 Blindern, NO-0315 Oslo, Norway
[49] Department of Astronomy and Astrophysics, University of California, Santa Cruz, CA 95064, USA
[50] Center for Astrophysical Surveys, National Center for Supercomputing Applications, 1205 West Clark Street, Urbana, IL 61801, USA
[51] School of Physics and Astronomy, University of Southampton, Southampton, SO17 1BJ, UK
[52] Instituto de Fisica Teorica UAM/CSIC, Universidad Autonoma de Madrid, 28049 Madrid, Spain
[53] Department of Astronomy, University of Illinois at Urbana-Champaign, 1002 West Green Street, Urbana, IL 61801, USA
[54] Department of Astronomy, University of Geneva, ch. d'Écogia 16, CH-1290 Versoix, Switzerland
[55] Santa Cruz Institute for Particle Physics, Santa Cruz, CA 95064, USA
[56] Center for Cosmology and Astro-Particle Physics, The Ohio State University, Columbus, OH 43210, USA
[57] Department of Physics, The Ohio State University, Columbus, OH 43210, USA
[58] ASTRAVEO LLC, P.O. Box 1668, Gloucester, MA 01931, USA
[59] Applied Materials Inc., 35 Dory Road, Gloucester, MA 01930, USA
[60] Department of Physics, University of Namibia, 340 Mandume Ndemufayo Avenue, Pionierspark, Windhoek, Namibia
[61] Lawrence Berkeley National Laboratory, 1 Cyclotron Road, Berkeley, CA 94720, USA
[62] TMT International Observatory, 100 West Walnut Street, Pasadena, CA 91124, USA
[63] California Institute of Technology, 1200 East California Boulevard, Pasadena, CA 91125, USA
[64] Australian Astronomical Optics, Macquarie University, North Ryde, NSW 2113, Australia
[65] Lowell Observatory, 1400 Mars Hill Road, Flagstaff, AZ 86001, USA
[66] Sydney Institute for Astronomy, School of Physics, A28, The University of Sydney, NSW 2006, Australia
[67] Department of Astronomy and Astrophysics, University of Toronto, 50 St. George Street, Toronto, ON M5S 3H4, Canada
[68] Centre for Gravitational Astrophysics, College of Science, The Australian National University, ACT 2601, Australia
[69] Department of Astronomy, The Ohio State University, Columbus, OH 43210, USA
[70] LPSC Grenoble—53, Avenue des Martyrs 38026 Grenoble, France
[71] Institució Catalana de Recerca i Estudis Avançats, E-08010 Barcelona, Spain
[72] Max Planck Institute for Extraterrestrial Physics, Giessenbachstrasse, 85748 Garching, Germany
[73] Perimeter Institute for Theoretical Physics, 31 Caroline Street North, Waterloo, ON N2L 2Y5, Canada
[74] School of Mathematics and Physics, University of Surrey, Guildford, Surrey, GU2 7XH, UK
[75] Observatório Nacional, Rua Gal. José Cristino 77, Rio de Janeiro, RJ—20921-400, Brazil
[76] Graduate Institute of Astronomy, National Central University, 300 Jhongda Road, 32001 Jhongli, Taiwan
[77] Hamburger Sternwarte, Universität Hamburg, Gojenbergsweg 112, 21029 Hamburg, Germany
[78] Ruhr University Bochum, Faculty of Physics and Astronomy, Astronomical Institute, 44780 Bochum, Germany
[79] Department of Physics, University of Genova and INFN, Via Dodecaneso 33, 16146, Genova, Italy
[80] Laboratoire de physique des 2 infinis Irène Joliot-Curie, CNRS Université Paris-Saclay, Bât. 100, F-91405 Orsay Cedex, France
[81] Department of Physics and Astronomy, Pevensey Building, University of Sussex, Brighton, BN1 9QH, UK
[82] Department of Physics, Baylor University, One Bear Place #97316, Waco, TX 76798-7316, USA
[83] Centro de Investigaciones Energéticas, Medioambientales y Tecnológicas (CIEMAT), Madrid, Spain
[84] Austin Peay State University, Department of Physics, Engineering and Astronomy, P.O. Box 4608, Clarksville, TN 37044, USA
[85] Physics Department, Lancaster University, Lancaster, LA1 4YB, UK
[86] University of Zurich, Physics Institute, Winterthurerstrasse 190/Building 36, 8057 Zürich, Switzerland
[87] Computer Science and Mathematics Division, Oak Ridge National Laboratory, Oak Ridge, TN 37831, USA
[88] Aix Marseille Univ, CNRS/IN2P3, CPPM, Marseille, France
[89] Centre for Space Studies, American Public University System, 111 West Congress Street, Charles Town, WV 25414, USA
[90] Department of Physics, Stanford University, 382 Via Pueblo Mall, Stanford, CA 94305, USA
[91] Universitäts-Sternwarte, Fakultät für Physik, Ludwig-Maximilians Universität München, Scheinerstr. 1, 81679 München, Germany
Received 2024 January 8; revised 2024 March 18; accepted 2024 March 28; published 2024 October 1

Abstract

We present cosmological constraints from the sample of Type Ia supernovae (SNe Ia) discovered and measured during the full 5 yr of the Dark Energy Survey (DES) SN program. In contrast to most previous cosmological samples, in which SNe are classified based on their spectra, we classify the DES SNe using a machine learning algorithm applied to their light curves in four photometric bands. Spectroscopic redshifts are acquired from a dedicated follow-up survey of the host galaxies. After accounting for the likelihood of each SN being an SN Ia, we find 1635 DES SNe in the redshift range $0.10 < z < 1.13$ that pass quality selection criteria sufficient to constrain cosmological parameters. This quintuples the number of high-quality $z > 0.5$ SNe compared to the previous leading compilation of Pantheon+ and results in the tightest cosmological constraints achieved by any SN data set to date. To derive cosmological constraints, we combine the DES SN data with a high-quality external low-redshift sample consisting of 194 SNe Ia spanning $0.025 < z < 0.10$. Using SN data alone and including systematic uncertainties, we find $\Omega_{\rm M} = 0.352 \pm 0.017$ in flat ΛCDM. SN data alone now require acceleration ($q_0 < 0$ in ΛCDM) with over 5σ confidence. We find $(\Omega_{\rm M}, w) = (0.264^{+0.074}_{-0.096}, -0.80^{+0.14}_{-0.16})$ in flat wCDM. For flat w_0w_aCDM, we find $(\Omega_{\rm M}, w_0, w_a) = (0.495^{+0.033}_{-0.043}, -0.36^{+0.36}_{-0.30}, -8.8^{+3.7}_{-4.5})$, consistent with a constant equation of state to within

~2σ. Including Planck cosmic microwave background, Sloan Digital Sky Survey baryon acoustic oscillation, and DES 3×2pt data gives $(\Omega_M, w) = (0.321 \pm 0.007, -0.941 \pm 0.026)$. In all cases, dark energy is consistent with a cosmological constant to within ~2σ. Systematic errors on cosmological parameters are subdominant compared to statistical errors; these results thus pave the way for future photometrically classified SN analyses.

Unified Astronomy Thesaurus concepts: Cosmology (343); Type Ia supernovae (1728); Dark energy (351); Dark matter (353)

1. Introduction

The standard cosmological model posits that the energy density of the Universe is dominated by dark components that have not been detected in terrestrial experiments and thus do not appear in the standard model of particle physics. Known as cold dark matter and dark energy, their study represents an opportunity to deepen our understanding of fundamental physics.

The Dark Energy Survey (DES) was conceived to characterize the properties of dark matter and dark energy with unprecedented precision and accuracy through four primary observational probes (The Dark Energy Survey Collaboration 2005; J. P. Bernstein et al. 2012; Dark Energy Survey Collaboration 2016; O. Lahav et al. 2020). One of these four probes is the Hubble diagram (redshift–distance relation) for Type Ia supernovae (SNe Ia), which act as standardizable candles (B. W. Rust 1974; I. P. Pskovskii 1977; M. M. Phillips et al. 1999) to constrain the history of the cosmic expansion rate. To implement this probe, the DES SN survey was designed to provide the largest, most homogeneous sample of high-redshift SNe ever discovered. The two papers that first presented evidence for the accelerated expansion of the Universe (A. G. Riess et al. 1998; S. Perlmutter et al. 1999) used a total of 52 high-redshift SNe with sparsely sampled light-curve measurements in one or two optical passbands. Building on two decades of subsequent improvements in SN surveys and analysis, we present here the cosmological constraints using the full 5 yr DES SN data set, consisting of well-sampled, precisely calibrated light curves for 1635 new high-redshift SNe observed in four bands: g, r, i, and z.

For the last decade, SN Ia cosmology constraints have largely come from combining data from many surveys. The recent Pantheon+ analysis (D. Brout et al. 2022a; D. Scolnic et al. 2022) combined three separate mid-z samples ($0.1 < z < 1.0$), 11 different low-z samples ($z < 0.1$), and four separate high-z samples ($z > 1.0$), each with different photometric systems and selection functions (R. L. Gilliland et al. 1999; A. G. Riess et al. 2001, 2004, 2007; M. Hicken et al. 2009; M. Sullivan et al. 2011; M. Hicken et al. 2012; N. Suzuki et al. 2012; M. Ganeshalingam et al. 2013; M. Betoule et al. 2014; R. J. Foley et al. 2017; K. Krisciunas et al. 2017; A. G. Riess et al. 2018; M. Sako et al. 2018; D. Brout et al. 2019b; M. Smith et al. 2020a). The DES sample, which rivals in number the entirety of Pantheon+, does not have the low-redshift ($z < 0.1$) coverage to completely remove the need for external low-z samples, but at higher redshift, it enables us to replace a heterogeneous mix of samples with a homogeneous sample of high-quality, well-calibrated light curves.

A key aim of the DES analysis was to minimize systematic (relative to statistical) errors to enable a robust analysis. M. Vincenzi et al. (2024) show that our error budget is dominated by statistical uncertainty, in contrast to most SN cosmology analyses of the last decade, for which the systematic uncertainties equaled or exceeded the statistical uncertainties (M. Betoule et al. 2014; D. M. Scolnic et al. 2018; Dark Energy Survey Collaboration 2019). We also highlight that the most critical sources of systematics are those related to the lack of a homogeneous and well-calibrated low-z sample.

As the DES sample enables an SN Ia measurement of cosmological parameters that is largely independent of previous SN cosmology analyses, we have been careful to “blind” our analysis (see Section 2.3). The analysis work described in M. Vincenzi et al. (2024), which stops just short of constraining cosmological parameters, was shared widely with the DES collaboration, evaluated, and approved before unblinding. Unblinding standards included multiple validation checks with simulations and a full accounting and explanation of the error budget. No elements of the analysis were changed after unblinding.

In this Letter, we review the analysis of the complete DES SN data set (as detailed in many supporting papers; see Figure 1) and present the cosmological results. An important advance on most previous analyses is that we use a photometrically classified rather than spectroscopically classified sample (A. Möller & T. de Boissiere 2020; H. Qu et al. 2021) and implement advanced techniques to classify SNe Ia and incorporate classification probabilities in the cosmological parameter estimation (M. Kunz et al. 2007, 2012; R. Hlozek et al. 2012). While this advance increases the complexity of the analysis, in this work and previous papers (A. Möller et al. 2022; M. Vincenzi et al. 2023), we show that the impact of non-SN Ia contamination due to photometric misclassification is well below the statistical uncertainty on the cosmological parameters, and this constitutes one of the key results of our analysis.

Combining our DES data with a low-redshift sample (see Section 2), we fit the Hubble diagram to test the standard cosmological model as well as multiple common extensions including spatial curvature, nonvacuum dark energy, and dark energy with an evolving equation-of-state parameter. In R. Camilleri et al. (2024), we present fits to more exotic models.

The structure of the Letter is as follows. We begin in Section 2 by describing the data set and its acquisition, reduction, calibration, and light-curve fitting. We summarize the models we test in Section 3 before presenting the results in Section 4; our discussion and conclusions follow in Section 5 and Section 6. The details of our data release, which includes the code needed to reproduce our results, appear in B. O. Sánchez (2024).

2. Data and Analysis

2.1. DES and Low-redshift SNe

Our primary data set is the full 5 yr of DES SNe, which we combine with a historical set of nearby SNe from CfA3 (M. Hicken et al. 2009), CfA4 (M. Hicken et al. 2012), Carnegie Supernova Project (CSP; K. Krisciunas et al. 2017; DR3), and the Foundation SN sample (R. J. Foley et al. 2017). We refer to the combined DES plus historical data set as DES-SN5YR.

DES-SN5YR analysis overview

Data:
- Calibration (Burke et al. 2018, Brout et al. 2022, Rykoff et al. 2023)
- SN photometry (Brout et al. 2019, Sanchez et al. 2024)
- SN spectroscopy (Smith et al. 2020a)
- DCR and chrom (Lasker et al. 2018, Lee&Acevedo et al. 2023)
- Host galaxy redshifts and properties (Lidman et al. 2020, Carr et al. 2021, Wiseman et al. 2020/2021, Kelsey et al. 2023)

Simulations:
- Survey selection effects (Kessler et al. 2019a, Vincenzi et al. 2020)
- SN Ia intrinsic and dust properties (Brout&Scolnic 2021, Popovic et al. 2021a/b, Wiseman et al. 2022) and rates (Wiseman et al. 2021)
- Contamination (Vincenzi et al. 2019/2020, Kessler et al. 2019b)

Analysis:
Pipeline and Overview (Hinton et al. 2020, Vincenzi et al. 2024)
- Light-curve fitting (Taylor et al. 2023)
- SN classification (Möller & de Boissière 2020, Qu et al. 2021, Vincenzi et al. 2021, Moller et al. 2022)
- "BEAMS" and bias corrections (Kessler & Scolnic 2017), unbinning the SN Hubble diagram (Brout et al. 2020, Kessler et al. 2023)
- Effects of host galaxy mismatch (Qu et al. 2023)
- Cosmological contour validation (Armstrong et al. 2023)

Cosmological results: **DES Collaboration 2024**
Testing non-standard cosmological models (Camilleri et al. 2024)

Figure 1. Overview of supporting papers for DES-SN5YR cosmological results.

The DES SN program was carried out over five seasons, August to February, from 2013 to 2018, during which we observed 10 ∼3 deg^2 fields with approximately weekly cadence in four bands (g, r, i, z). Eight of the fields were observed to a 5σ depth of ∼23.5 mag in all four bands (shallow fields) and two to a deeper limit of ∼24.5 mag (deep fields). See B. Flaugher et al. (2015) for a summary of the Dark Energy Camera, M. Smith et al. (2020a) for a summary of the SN program, and H. T. Diehl et al. (2016, 2018) for observational details.

The DES SNe were discovered via difference imaging (R. Kessler et al. 2015) based on the method of C. Alard & R. H. Lupton (1998). DES images are calibrated following the forward global calibration method (D. L. Burke et al. 2018; I. Sevilla-Noarbe et al. 2021; E. S. Rykoff 2023), and both DES and low-z samples are recalibrated as part of the SuperCal-Fragilistic cross-calibration effort described in D. Brout et al. (2022b). SN fluxes are determined using scene-modeling photometry (D. Brout et al. 2019b); we include corrections from spectral energy distribution (SED) variations (D. L. Burke et al. 2018; J. Lasker et al. 2019) and from differential chromatic refraction and wavelength-dependent seeing (J. Lee et al. 2023). We estimate the overall accuracy of our calibrated photometry to be $\lesssim$5 mmag. Host galaxies are assigned following the directional light radius method (M. Sullivan et al. 2006; R. R. Gupta et al. 2016; H. Qu et al. 2023), and host galaxy properties are determined as described by L. Kelsey et al. (2023) based on M. Fioc & B. Rocca-Volmerange (1999) using deep coadded images by P. Wiseman et al. (2020). Host galaxy spectroscopic redshifts are obtained primarily within the OzDES program (F. Yuan et al. 2015; M. J. Childress et al. 2017; C. Lidman et al. 2020). The final data release of the photometry of ∼20,000 candidates, redshifts of hosts, and host galaxy properties is presented in B. O. Sánchez (2024).

We apply strict quality cuts to this sample of candidates to select our final high-quality sample for the Hubble diagram. The same quality cuts were applied to both the low-z sample and the DES SNe. First, we require a spectroscopic redshift of the host galaxy, good light-curve coverage (at least two detections with signal-to-noise ratio > 5 in two different bands), and a well-converged light-curve fit using the SALT3 model[92] (W. D. Kenworthy et al. 2021; G. Taylor et al. 2023); this reduces the DES sample size to 3621. Additional requirements include light-curve parameters (stretch and color) within the normal range for SNe Ia, a well-constrained time of peak brightness (uncertainty less than 2 days), good SALT3 fit probability, and valid distance bias correction from our simulation (see Table 4 of M. Vincenzi et al. 2024 for more details). Our final Hubble diagram sample includes 1635 SNe, of which 1499 have a machine learning probability of being a Type Ia greater than 50% (see Section 2.2). Note that we do not perform a cut on this machine learning probability; rather, we use it in the BEAMS formalism that produces our Hubble diagram and to weight the SN distance uncertainties in the fits to the final Hubble diagram (R. Kessler et al. 2023). The set of all DES light curves is visualized in Figure 2.

Since we focus on minimizing potential systematic errors, we only use the best-calibrated, most homogeneous sample of low-z SNe Ia. To reduce the impact of peculiar velocity uncertainties, we remove SNe with $z < 0.025$. We furthermore combine only a subset of the available low-redshift samples: CfA3 and 4, CSP, and Foundation SNe, which are the four largest low-z samples with the most well-understood photometric calibration. Our low-z sample thus totals 194 SNe with $z < 0.1$; this can be compared to Pantheon+, for which the low-z sample was almost 4 times larger (741 SNe at $z < 0.1$). We have thus exchanged the statistical constraining power of more low-z SNe for better control of systematics. The redshift distribution of our sample compared to the compilation of historical samples in Pantheon+ is shown in Figure 3. To conclude, the final DES-SN5YR sample includes 1635 DES SNe and 194 low-z external SNe, for a total of 1829 SNe.

2.2. From Light Curves to Hubble Diagram

A critical step in the cosmology analysis is to convert each SN's light curve (magnitude versus time in multiple bands; see examples in Figure 2) to a single calibrated number representing its standardized magnitude and estimated distance modulus.

To achieve this, we use the SALT3 light-curve fitting model as presented in W. D. Kenworthy et al. (2021) and G. Taylor et al. (2023) and retrained in M. Vincenzi et al. (2024) to determine the light-curve fit parameters, the amplitude of the SN flux (x_0), stretch (x_1), and color (c). These fitted parameters are used to estimate the distance modulus, $\mu \equiv m - M$, using an adaptation of the Tripp equation (R. Tripp 1998) that includes a correction for observed correlations between SN Ia luminosity

[92] The SALT3 model consists of a spectral flux density as a function of phase and wavelength for SNe Ia. Its three components are M_0 describing the mean SN light curve, M_1 describing the deviations from M_0 that are correlated with light-curve width, and CL describing the color dependence. See Equation (1) of G. Taylor et al. (2023).

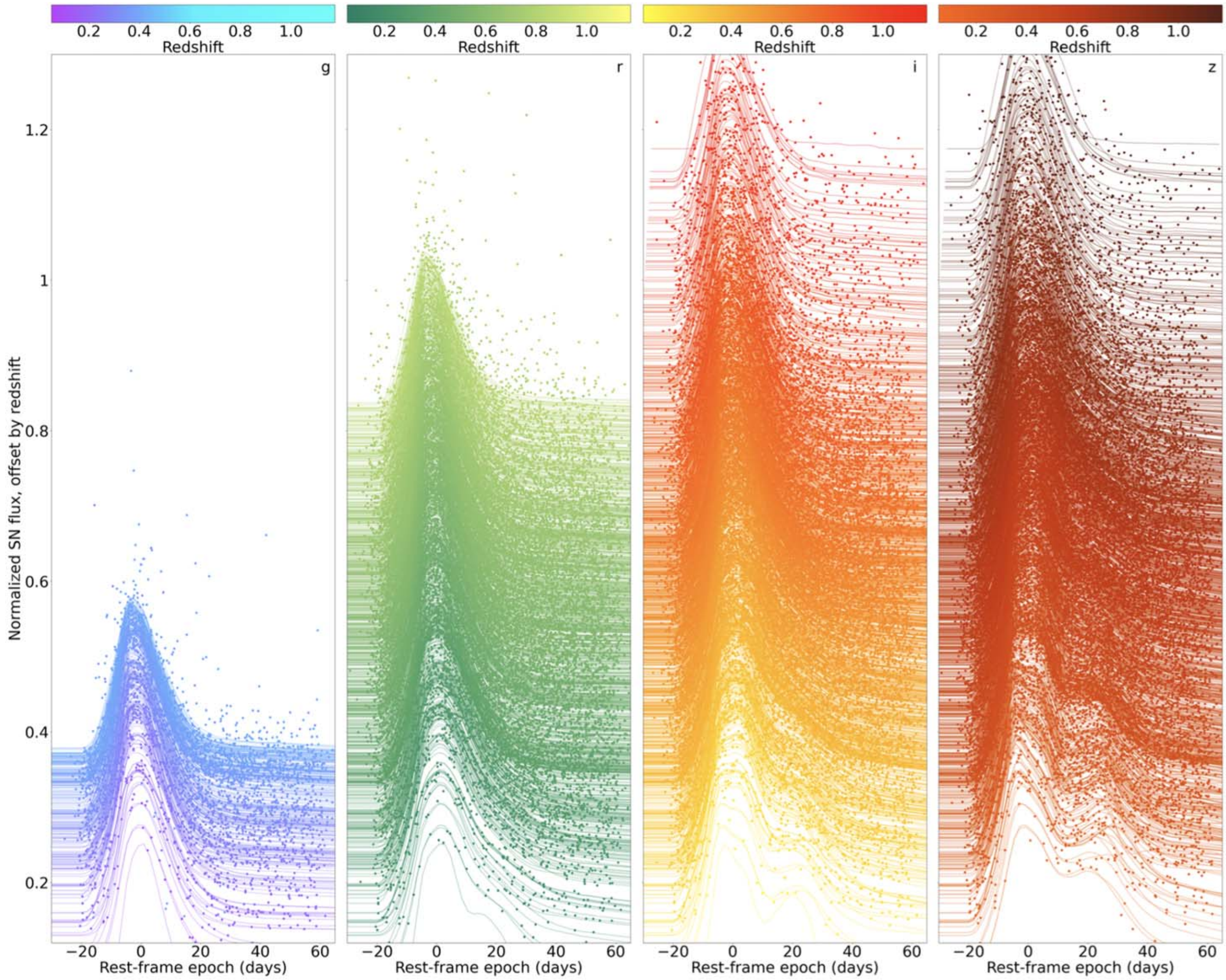

Figure 2. All DES light curves, showing observed magnitudes in the g, r, i, and z bands (left to right, respectively), normalized by the maximum brightness of each light curve and with the time axis de-redshifted to the rest frame. Each light curve has been arbitrarily offset by the redshift, with higher-redshift objects higher on the plot (as labeled on the vertical axis). Lines show best-fit SALT3 light-curve fits. The g-band and r-band light curves are not used above $z \sim 0.4$ and $z \sim 0.85$, respectively, because that corresponds to the redshifts at which the lower-wavelength limit of the SALT3 model (3500 Å in the rest frame) passes out of their observed wavelength ranges.

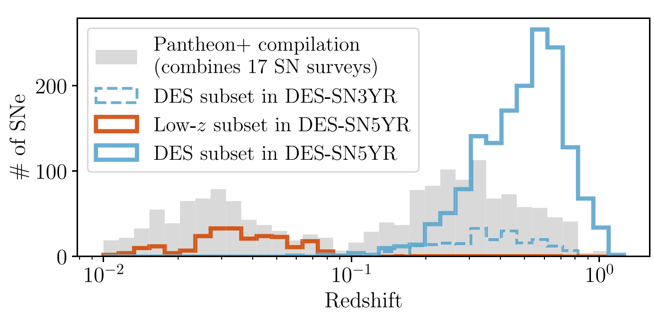

Figure 3. Histogram showing the redshift distribution of the DES-SN5YR sample, with new DES SNe in blue and our low-z sample in red. For comparison, the distribution of redshifts in the existing Pantheon+ sample is shown in gray (D. Brout et al. 2022a), which also includes the DES SNe from the DES-SN3YR analysis (blue dashed line). The 5 yr DES sample contains $\sim 4\times$ more SNe above $z \sim 0.4$ than the Pantheon+ compilation.

and host properties, $\gamma G_{\rm host} = \pm\gamma/2$. Here γ is the size of the step and $G_{\rm host}$ is the property of the host galaxy that is used to determine the step (i.e., mass or color); the sign is + if $G_{\rm host}$ is above the step or – if below. This correction has historically been described as a "mass step," but we also consider the possibility that it is a "color step" (see Section 2.2 of M. Vincenzi et al. 2024),

$$\mu_{{\rm obs},i} = m_{x,i} + \alpha x_{1,i} - \beta c_i + \gamma G_{{\rm host},i} - M - \Delta\mu_{{\rm bias},i}, \quad (1)$$

where $m_x = -2.5\log_{10}(x_0)$.[93] The constants α, β, and γ are global parameters determined from the likelihood analysis of all the SNe on the Hubble diagram, while the terms subscripted by i refer to parameters of individual SNe. We find $\alpha = 0.161 \pm 0.001$, $\beta = 3.12 \pm 0.03$, and $\gamma = 0.038 \pm 0.007$. We marginalize over the absolute magnitude M (see Section 3). The final term in Equation (1) accounts for selection effects, Malmquist bias, and light-curve fitting bias.

[93] Following J. Marriner et al. (2011), we replace the traditional m_B notation with m_x, because in the SALT2 and SALT3 models, the amplitude term, x_0, is not related to any particular filter band.

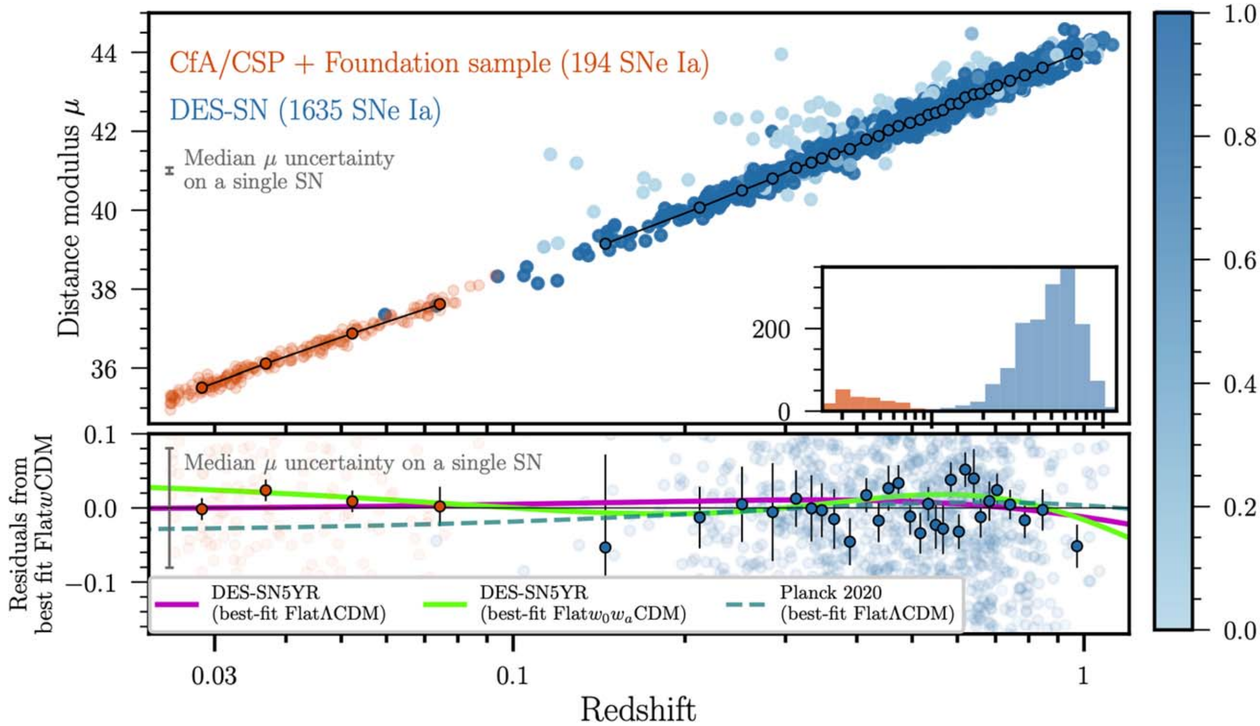

Figure 4. Hubble diagram of DES-SN5YR. We show both the single SN events and the redshift-binned SN distance moduli. Redshift bins are adjusted so that each bin has the same number of SNe (∼50). The 1635 new DES SNe are in blue, and in the upper panel, they are shaded by their probability of being a Type Ia; most outliers are likely contaminants (pale blue). The inset shows the number of SNe as a function of redshift (same z range as the main plot). The lower panel shows the difference between the data and the best-fit flat wCDM model from DES-SN5YR alone (third result in Table 2) and overplots three other best-fit cosmological models —the flat ΛCDM model from DES-SN5YR alone (magenta line; first result in Table 2), the flat w_0w_aCDM model from DES-SN5YR alone (green line; fourth result in Table 2), and the Planck 2020 flat ΛCDM model without SN data (dashed line; $\Omega_{\rm M}^{\rm Planck} = 0.317 \pm 0.008$).

The nuisance parameters and $\Delta\mu_{{\rm bias},i}$ term in Equation (1) are determined using the "BEAMS with Bias Corrections" (BBC) framework (R. Kessler & D. Scolnic 2017). In particular, bias corrections $\Delta\mu_{{\rm bias},i}$ are estimated from a large simulation of our sample. The simulation models the rest-frame SN Ia SED at all phases, SN correlations with host galaxy properties, SED reddening through an expanding Universe, broadband *griz* fluxes, and instrumental noise (see Figure 1 in R. Kessler et al. 2019a). Using Equation (1), there remains an intrinsic scatter of ∼0.1 mag in the Hubble residuals. Following the numerous recent studies on understanding and modeling SN Ia dust extinction and progenitors (P. Wiseman et al. 2021, 2022; Chen et al. 2022; J. Duarte et al. 2023; M. Dixon et al. 2022; C. Meldorf et al. 2023), we model this residual scatter using the dust-based model from D. Brout & D. Scolnic (2021) and B. Popovic et al. (2023). In contrast to previously used models in Kessler et al. (2013), the D. Brout & D. Scolnic (2021) model accurately models the Hubble residual bias and scatter as a function of the fitted SALT2 color (see Figure 5 in M. Vincenzi et al. 2024 and Figure 6 in D. Brout & D. Scolnic 2021). Due to uncertainties in the fitted dust parameters (B. Popovic et al. 2023), this intrinsic scatter model remains the largest source of systematic uncertainty from the simulation.

As we do not spectroscopically classify the SNe and thus expect contamination from core-collapse SNe, we perform machine learning light-curve classification on the sample following A. Möller et al. (2022) and M. Vincenzi et al. (2023). We implement two advanced machine learning classifiers, SuperNNova (A. Möller & T. de Boissiere 2020) and SCONE (H. Qu et al. 2021), and use state-of-the-art simulations to model contamination (estimated to be ∼6.5%; see Table 10 and Section 7.1.5 of M. Vincenzi et al. 2024). Classifiers are trained using core-collapse and peculiar SN Ia simulations based on M. Vincenzi et al. (2021) and state-of-the-art SED templates by R. Kessler et al. (2019b) and M. Vincenzi et al. (2019). These DES simulations are the first to robustly reproduce the contamination observed in the Hubble residuals (M. Vincenzi et al. 2021, 2024, Table 10).

For each SN, the trained classifiers assign a probability of being a Type Ia, and these probabilities are included within the BEAMS framework to marginalize over core-collapse contamination and produce the final Hubble diagram (R. Hlozek et al. 2012; M. Kunz et al. 2012). The final DES-SN5YR Hubble diagram is shown in Figure 4 and includes 1829 SNe.

As discussed in R. Kessler et al. (2023) and M. Vincenzi et al. (2024), the probability that each SN is a Type Ia ($P_{\rm Ia}$) is incorporated in the BBC fit and used to calculate a BEAMS probability, $P_{\rm B(Ia)}$ (see Equation (9) in R. Kessler et al. 2023). BEAMS probabilities are used to inflate distance uncertainties of likely contaminants by a factor $\propto 1/\sqrt{P_{\rm B(Ia)}}$ (see Equation (10) in M. Vincenzi et al. 2024). Therefore, the released Hubble diagram data include distance bias corrections and inflated distance uncertainties (see Appendix A), enabling users to fit the Hubble diagram without applying additional corrections. With this BEAMS uncertainty weight, we find 75 SNe with distance modulus uncertainties $\sigma_{\mu,i,{\rm final}} > 1$ mag and 1331 SNe with $\sigma_{\mu,i,{\rm final}} < 0.2$ mag.[94]

[94] Applying a binary-classification-based cut (SN Ia or not) is not optimal, as it assumes that the classification is perfect. However, we test the binary-cut-based approach by using only the 1499 SNe classified with $P_{\rm Ia} > 0.5$ and assuming they are a pure SN Ia sample. We show that the measured shift in w is small compared to the statistical uncertainties (Table 11 of M. Vincenzi et al. 2024).

M. Vincenzi et al. (2024) stop short of performing cosmological constraints but provide the corrected distance moduli μ along with their uncertainties σ_μ, redshifts for each SN, and a statistical+systematic covariance matrix C, which we describe further in Section 3.

P. Armstrong et al. (2023) present validation of the cosmological contours produced by our pipeline. Validation that our analysis pipeline is insensitive to the cosmological model assumed in our bias correction simulation appears in R. Camilleri et al. (2024).

2.3. Unblinding Criteria

Throughout our analysis, cosmological parameters estimated from *real data* were blinded. We validate our entire pipeline on detailed catalog-level simulations and examine the cosmological parameters estimated from *simulations* to test that the input cosmology is recovered. In addition to the many tests described in M. Vincenzi et al. (2024), the final unblinding criteria that our data passed were as follows.

1. *Accuracy of simulations.* The reduced χ^2 between the distribution of data and simulations across a variety of observables (redshift, SALT3 parameters and goodness of fit, maximum signal-to-noise ratio at peak, host stellar mass) is required to be between 0.7 and 3.0 (see Figures 3 and 4 of M. Vincenzi et al. 2024).
2. *Pipeline validation using DES simulations.* Demonstrate that our pipeline recovers the input cosmology. We produce 25 data-size simulated samples (statistically independent) assuming a flat ΛCDM Universe with a best-fit Planck value of $\Omega_{\rm M}$ and analyze them the same way as real data. We fit each Hubble diagram assuming a flat *w*CDM model with a Planck prior and find a mean bias of $w - w_{\rm true} \simeq 0.001 \pm 0.020$, where w is the mean value of the marginalized posterior of the dark energy equation-of-state parameter over the 25 samples and $w_{\rm true} = -1$ is the model value of that parameter input to the simulation.
3. *Validation of contours*. Ensuring that our uncertainty limits accurately represent the likelihood of the models (P. Armstrong et al. 2023).
4. *Independence of reference cosmology.* Ensuring that our results are sufficiently independent of cosmological assumptions that enter our bias correction simulations (R. Camilleri et al. 2024).

2.4. Combining SNe with Other Cosmological Probes

We combine the DES-SN5YR cosmological constraints with measurements from other complementary cosmological probes. In particular, we use the following.

1. Cosmic microwave background (CMB) measurements of the temperature and polarization power spectra (TTTEEE) presented by the Planck Collaboration (2020). We use the Python implementation of Planck's 2015 `Plik_lite` (H. Prince & J. Dunkley 2019).
2. Weak-lensing and galaxy clustering measurements from the DES3 × 2pt year 3 magnitude-limited (MagLim) lens sample; 3 × 2pt refers to the simultaneous fit of three two-point correlation functions, namely, galaxy–galaxy, galaxy–lensing, and lensing–lensing correlations (Dark Energy Survey Collaboration 2022, 2023).
3. Baryon acoustic oscillation (BAO) measurements as presented in the extended Baryon Oscillation Spectroscopic Survey (eBOSS) paper (K. S. Dawson et al. 2016; S. Alam et al. 2021), which adds the BAO results from Sloan Digital Sky Survey (SDSS)-IV (M. R. Blanton et al. 2017) to earlier SDSS BAO data. Specifically, we use "BAO" to refer to the BAO-only measurements from the main galaxy sample (A. J. Ross et al. 2015), BOSS (SDSS-III; S. Alam et al. 2017), eBOSS LRG (J. E. Bautista et al. 2021), eBOSS ELG (A. de Mattia et al. 2021), eBOSS QSO (J. Hou et al. 2021), and eBOSS Lya (H. du Mas des Bourboux et al. 2020).

When combining these data, we run simultaneous Markov Chain Monte Carlo (MCMC) fits of the relevant data vectors. We present three combinations: the simplest CMB-dependent combination CMB+SN, a CMB-independent combination BAO+3 × 2pt+SN, and a combination of them all.

3. Models and Theory

We present cosmological results for the standard cosmological model—flat space with cold dark matter and a cosmological constant (flat ΛCDM)—and some basic extensions, such as relaxing the assumption of spatial flatness (ΛCDM), allowing for a constant equation-of-state parameter (w) of dark energy (flat *w*CDM), and including a linear parameterization for time-varying dark energy (flat w_0w_aCDM) in which the equation-of-state parameter is given by $w = w_0 + w_a(1 - a)$ (M. Chevallier & D. Polarski 2001; E. V. Linder 2003).

To calculate the theoretical distance as a function of redshift, we begin with the comoving distance,

$$R_0\chi(\bar{z}) = \frac{c}{H_0}\int_0^{\bar{z}} \frac{dz}{E(z)}, \tag{2}$$

where $\bar{z}$ is the redshift due to the expansion of the Universe, $E(z) \equiv H(z)/H_0$ is the normalized redshift-dependent expansion rate and is given for each cosmological model by the expression in Table 1, $R_0 = c/(H_0\sqrt{|\Omega_{\rm K}|})$ is the scale factor with dimensions of distance (where subscript 0 indicates its value at the present day), and $\Omega_{\rm K} \equiv 1 - \Omega_{\rm M} - \Omega_\Lambda$ is the curvature term. The dimensionless scale factor ($a \equiv R/R_0$) at the time of emission for an object with cosmological redshift $\bar{z}$ is $a = 1/(1 + \bar{z})$. The luminosity distance is given by

$$D_{\rm L}(z_{\rm obs}, \bar{z}) = (1 + z_{\rm obs})R_0 S_k(\chi(\bar{z})), \tag{3}$$

where $z_{\rm obs}$ is the observed redshift, and the curvature is captured by $S_k(\chi) = \sin\chi$, χ, and $\sinh\chi$ for closed ($\Omega_{\rm K} < 0$), flat ($\Omega_{\rm K} = 0$), and open ($\Omega_{\rm K} > 0$) universes, respectively.[95]

To compare data (Equation (1)) to theory, we calculate the theoretical distance modulus, which is dependent on the set of cosmological parameters we are interested in (Θ, given in the right column of Table 1),

$$\mu(z, \Theta) = 5\log_{10}(D_{\rm L}(z, \Theta)/1\ {\rm Mpc}) + 25. \tag{4}$$

We compute the difference between data and theory for every ith SN, $\Delta\mu_i = \mu_{{\rm obs},i} - \mu(z_i, \Theta)$, and find the minimum of

$$\chi^2 = \Delta\mu_i \mathcal{C}_{ij}^{-1} \Delta\mu_j^T\,, \tag{5}$$

[95] When $\Omega_{\rm K} = 0$, the term $R_0S_k(\chi)$ becomes $R_0\chi$ and can be calculated directly from Equation (2), bypassing the infinite R_0.

Table 1
Variations on the Standard Cosmological Model that Are Tested in This Letter, Their Friedmann Equations, and the Free Parameters in the Fit

Cosmological Model	Friedmann Equation: $E(z) = H(z)/H_0 =$	**Fit Parameters** Θ
Flat ΛCDM	$[\Omega_M(1+z)^3 + (1-\Omega_M)]^{1/2}$	Ω_M
ΛCDM	$[\Omega_M(1+z)^3 + \Omega_\Lambda + (1-\Omega_M-\Omega_\Lambda)(1+z)^2]^{1/2}$	Ω_M, Ω_Λ
Flat wCDM	$[\Omega_M(1+z)^3 + (1-\Omega_M)(1+z)^{3(1+w)}]^{1/2}$	Ω_M, w
Flat w_0w_aCDM	$[\Omega_M(1+z)^3 + (1-\Omega_M)(1+z)^{3(1+w_0+w_a)}e^{-3w_a z/(1+z)}]^{1/2}$	Ω_M, w_0, w_a

where $\mathcal{C}^{-1}$ is the inverse covariance matrix (including both statistical and systematic errors) of the $\Delta\mu$ vector (see Section 3.6 of M. Vincenzi et al. 2024).

The uncertainty covariance matrix includes a diagonal statistical term (discussed in Section 2.2) and a systematic term. The systematic covariance matrix is built following the approach in A. Conley et al. (2011) and accounts for systematics such as calibration, intrinsic scatter, and redshift corrections (see Table 6 of M. Vincenzi et al. 2024). Each element of the covariance matrix expresses the covariance between two of the SNe in the sample. The covariance matrix has the dimensions of the number of SNe, $N_{\rm SNe} \times N_{\rm SNe}$, and we follow the formalism introduced by D. Brout et al. (2021) and R. Kessler et al. (2023).

Finally, the absolute magnitude of SNe Ia (M) and the H_0 parameter (which appears in the luminosity distance) are completely degenerate; therefore, they are combined in the single parameter $\mathcal{M} = M + 5\log_{10}(c/H_0)$. All of our cosmology results are marginalized over this term. Therefore, the value of H_0 has no impact on the fitting of our cosmological results, and we do not constrain H_0. While $\mathcal{M}$ has no impact on cosmology fitting, a precise value is needed to simulate bias corrections. The $\mathcal{M}$ uncertainty is below 0.01, resulting in a negligible impact on bias corrections (D. Brout et al. 2022a; R. Camilleri et al. 2024).

4. Results

With the new DES high-redshift SN sample, we can put strong constraints on cosmological models. Of particular interest is whether dark energy is consistent with a cosmological constant or whether its density and/or equation-of-state parameter varies over the wide redshift range of our sample. The results of our cosmological fits are outlined in this section and summarized in Table 2, and their implications are explored in Section 5.

We estimate cosmological constraints using MCMC methods as implemented the CosmoSIS framework (J. Zuntz et al. 2015), the samplers `emcee` for best fits (D. Foreman-Mackey et al. 2013), and PolyChord for tension metrics (W. J. Handley et al. 2015),[96] except for fits that include BAO+3 × 2pt, which are calculated using PolyChord for both best fit and tensions.[97]

For all fits, we present the median of the marginalized posterior and cumulative 68.27% confidence intervals. The chains and code (with the flexibility to test other statistical choices) are publicly available (see Appendix A). Figures 5, 6, 7, and 8 all present the joint probability contours for 68.3% and 95.5%.

4.1. Constraints on Cosmological Parameters

4.1.1. Flat ΛCDM

For the simplest parameterization, flat ΛCDM, Ω_M is the only free parameter. We show the probability density function of this constraint for DES-SN5YR in Figure 5; we measure a value of $\Omega_M = 0.352 \pm 0.017$. We also show the probability distribution of the Planck Collaboration (2020) measurement of $\Omega_M^{\rm Planck} = 0.317 \pm 0.008$. These are approximately[98] 2σ apart but not in significant tension, as discussed in Section 4.2.

Combining DES-SN5YR with Planck CMB gives $\Omega_M = 0.338^{+0.016}_{-0.014}$, while combining with BAO+3 × 2pt gives $\Omega_M = 0.330^{+0.011}_{-0.010}$. Combining all three gives $\Omega_M = 0.315 \pm 0.007$. Interestingly, the combination of all data sets (red in Figure 5) gives a lower Ω_M than any of the other combinations. The reason can be seen in Figure 6, where all constraints cross the flat Universe line to the upper left of any individual best fit.

4.1.2. ΛCDM

Fitting DES-SN5YR to the ΛCDM model, we find $(\Omega_M, \Omega_\Lambda) = (0.291^{+0.063}_{-0.065},\ 0.55 \pm 0.17)$, consistent with a flat Universe ($\Omega_K = 0.16 \pm 0.16$); see Figure 6. Combining DES-SN5YR with BAO+3 × 2pt is also consistent with a flat Universe, with uncertainties on Ω_K reduced to $\sim\pm 0.034$, while the combination with Planck gives $\Omega_K = 0.010 \pm 0.005$. The combination of all three gives $\Omega_K = 0.002^{+0.004}_{-0.003}$.

4.1.3. Flat wCDM

Fitting DES-SN5YR to the flat wCDM model, we measure $(\Omega_M,\ w) = (0.264^{+0.074}_{-0.096},\ -0.80^{+0.14}_{-0.16})$; see Figure 7. This is consistent with a cosmological constant (within 2σ), although our data favor a w value that is slightly larger than -1.

The $w - \Omega_M$ contours from SNe alone are highly non-Gaussian with a curved "banana"-shaped degeneracy. The best-fit value for w or Ω_M is thus an insufficient summary of the SN information, as a small shift along the degeneracy direction can result in large shifts in the best-fit values. To address this issue, in R. Camilleri et al. (2024), we introduce a new parameter, $Q_H(z) \equiv -\ddot{a}/(aH_0^2) \equiv q(H/H_0)^2$. This combination of the deceleration parameter q and the Friedmann equation H/H_0 follows the curve of the degeneracy in the w–Ω_M plane. Therefore, measuring $Q_H(z)$ summarizes the SN information in

[96] For each `emcee` fit, we use a number of walkers that is at least twice the number of parameters and ensure that the number of samples in the chain is greater than 50 times the autocorrelation function, τ ($N_{\rm samples}/\tau > 50$). For each PolyChord fit, we use a minimum of 60 live points, 30 repeats, and an evidence tolerance requirement of 0.1 (except for ΛCDM with all data sets combined, for which we accepted a slightly weaker tolerance because convergence was too slow). When combining with other data sets, we run simultaneous MCMC chains including all relevant data vectors. Flat priors that encapsulate at least the 99.7% confidence region were chosen in each case, and we summarize those priors in Appendix B.

[97] The main advantage of `emcee` is that it gives a slightly more accurate best-fit χ^2 than PolyChord. However, we decided that the tiny improvement in accuracy was not worth the environmental impact (A. R. H. Stevens et al. 2020) of the extra compute time (which was substantial for the many-data-set fits).

[98] The distribution of points around the Hubble diagram is not perfectly Gaussian, as it is skewed due to lensing magnification and non-SN-Ia contamination. This means that the σ values (especially at high σ) are only approximate.

Table 2
Results for Four Different Cosmological Models, Sorted into Sections for Different Combinations of Observational Constraints

	Ω_M	Ω_K	w_0	w_a	χ^2/dof
DES-SN5YR (No External Priors)					
Flat ΛCDM	0.352 ± 0.017	⋯	⋯	⋯	$1649/1734 = 0.951$
ΛCDM	$0.291^{+0.063}_{-0.065}$	0.16 ± 0.16	⋯	⋯	$1648/1733 = 0.951$
Flat wCDM	$0.264^{+0.074}_{-0.096}$	⋯	$-0.80^{+0.14}_{-0.16}$	⋯	$1648/1733 = 0.951$
Flat w_0w_aCDM	$0.495^{+0.033}_{-0.043}$	⋯	$-0.36^{+0.36}_{-0.30}$	$-8.8^{+3.7}_{-4.5}$	$1641/1732 = 0.948$
DES-SN5YR + Planck 2020					
Flat ΛCDM	$0.338^{+0.016}_{-0.014}$	⋯	⋯	⋯	$2237/2349 = 0.952$
ΛCDM	$0.359^{+0.014}_{-0.016}$	0.010 ± 0.005	⋯	⋯	$2231/2348 = 0.950$
Flat wCDM	$0.337^{+0.013}_{-0.011}$	⋯	$-0.955^{+0.032}_{-0.037}$	⋯	$2234/2348 = 0.951$
Flat w_0w_aCDM	$0.325^{+0.016}_{-0.012}$	⋯	-0.73 ± 0.11	$-1.17^{+0.55}_{-0.62}$	$2231/2347 = 0.951$
DES-SN5YR + SDSS BAO and DES Y3 3 × 2pt					
Flat ΛCDM	$0.330^{+0.011}_{-0.010}$	⋯	⋯	⋯	$2194/2212 = 0.992$
ΛCDM	$0.327^{+0.012}_{-0.011}$	0.030 ± 0.034	⋯	⋯	$2194/2211 = 0.992$
Flat wCDM	$0.323^{+0.011}_{-0.010}$	⋯	$-0.922^{+0.035}_{-0.037}$	⋯	$2188/2211 = 0.989$
Flat w_0w_aCDM	0.334 ± 0.012	⋯	$-0.778^{+0.088}_{-0.080}$	$-0.93^{+0.46}_{-0.53}$	$2191/2210 = 0.992$
DES-SN5YR + Planck 2020 + SDSS BAO and DES Y3 3 × 2pt					
Flat ΛCDM	0.315 ± 0.007	⋯	⋯	⋯	$2791/2828 = 0.987$
ΛCDM	$0.318^{+0.011}_{-0.010}$	$0.002^{+0.004}_{-0.003}$	⋯	⋯	$2825/2827 = 0.999$
Flat wCDM	0.321 ± 0.007	⋯	-0.941 ± 0.026	⋯	$2785/2827 = 0.985$
Flat w_0w_aCDM	0.325 ± 0.008	⋯	$-0.773^{+0.075}_{-0.067}$	$-0.83^{+0.33}_{-0.42}$	$2782/2826 = 0.984$

Note. These are the medians of the marginalized posterior with 68.27% integrated uncertainties ("cumulative" option in ChainConsumer). For each fit, we also show the χ^2/dof as a measure of the goodness of fit.

a single, almost degeneracy-free value.[99] One has to choose the redshift at which one quotes $Q_H(z)$ to best match the angle of the degeneracy for the redshift range of the sample. We find $Q_H(z = 0.2) = -0.340 \pm 0.032$ using DES-SN5YR only (see R. Camilleri et al. 2024). This Q_H value can be used to roughly approximate the DES-SN5YR results and characterize the constraining power without the need for a full fit to the Hubble diagram.

The degeneracy in the $w-\Omega_M$ plane is broken by combining SNe with external probes. Combining with Planck, we measure $(\Omega_M,\ w) = (0.337^{+0.013}_{-0.011},\ -0.955^{+0.032}_{-0.037})$, again within 2σ of a cosmological constant. Planck alone provides only a loose constraint on the equation-of-state parameter of dark energy, $w^{\rm Planck} = -1.51^{+0.27}_{-0.18}$; combining with DES-SN5YR reduces the uncertainty significantly due to the different degeneracy direction, demonstrating the combined constraining power of these two complementary probes.

Combining DES-SN5YR with BAO+3 × 2pt, we find $w = -0.922^{+0.035}_{-0.037}$, slightly over 2σ from the cosmological constant. This data combination demonstrates that these late-Universe probes alone provide constraints that are consistent with—and of comparable constraining power to—the combination of SN and CMB data. The full combination of all data sets gives $w = -0.941 \pm 0.026$.

[99] Similar to the S_8 parameter used in lensing studies to approximate σ_8–Ω_M constraints.

4.1.4. Flat w_0w_aCDM

Fitting DES-SN5YR alone to the flat w_0w_aCDM model gives an equation of state that is slightly over 2σ from a cosmological constant, marginally preferring a time-varying dark energy $(\Omega_M,\ w_0,\ w_a) = (0.495^{+0.033}_{-0.043},\ -0.36^{+0.36}_{-0.30},\ -8.8^{+3.7}_{-4.5})$; see Figure 8.

Combining DES-SN5YR and the CMB, we find $(\Omega_M,\ w_0,\ w_a) = (0.325^{+0.016}_{-0.012},\ -0.73 \pm 0.11,\ -1.17^{+0.55}_{-0.62})$, which again deviates slightly from the cosmological constant. The same trend is seen when combining with BAO+3 × 2pt and with all data combined. The negative w_a means that the dark energy equation-of-state parameter is *increasing* with time (sometimes referred to as a "thawing" model).

4.2. Goodness of Fit and Tension

4.2.1. χ^2 per Degree of Freedom

To assess whether our best fits are good fits, we calculate the χ^2 per degree of freedom (dof) for all our data set and model combinations; see the last column of Table 2. The χ^2 we use for this test is the maximum likelihood of the entire parameter space, not the marginalized best fit for each parameter.

The number of dof is the number of data points minus the number of parameters that are common to all data sets (i.e., the cosmological parameters of interest). The number of data points added by the CMB, BAO, and 3 × 2pt is, respectively, 615, 8, and 471. Due to our treatment of contamination (by inflating the uncertainties of SNe with a low $P_{\rm Ia}$), we approximate the effective number of data points in the DES-

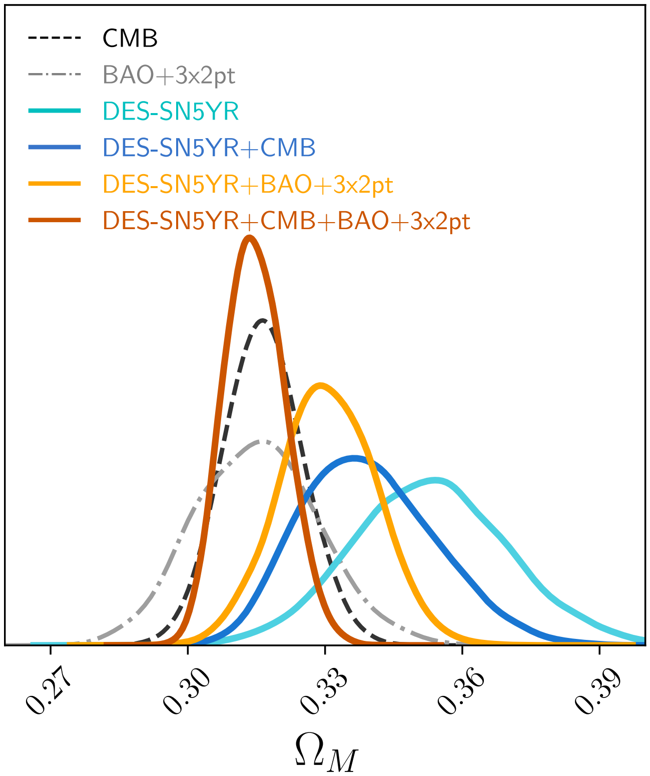

Figure 5. Constraints on matter density in the flat ΛCDM model from DES-SN5YR only (cyan), DES-SN5YR combined with CMB constraints from Planck Collaboration (2020; blue), DES-SN5YR combined with BAO $+3 \times 2$pt (orange), and all probes combined (DES-SN5YR+BAO+3×2pt and CMB constraints; red). CMB constraints only and BAO+3×2pt constraints alone are also shown for comparison (dashed and dotted–dashed, respectively).

SN5YR sample by $\sum P_{\mathrm{B(Ia)}} = 1735$ (rather than the total number of data points, 1829).

Ideally, a good fit should have $\chi^2/\mathrm{dof} \sim 1.0$. The slightly low χ^2/dof for the DES-SN5YR data arises because $\sum P_{\mathrm{B(Ia)}}$ only approximates the number of dof, and the same behavior is also seen in simulations.

4.2.2. Suspiciousness

Suspiciousness, S (W. Handley & P. Lemos 2019), is closely related to the Bayes ratio, R,[100] and can be used to assess whether different data sets are consistent. However, while the Bayes ratio has been shown to be prior-dependent (W. Handley & P. Lemos 2019), with wider prior widths boosting the confidence, suspiciousness is prior-independent. Therefore, suspiciousness is ideal for cases such as ours where we have chosen deliberately wide and uninformative priors (P. Lemos et al. 2021, Section 4.2). R. Trotta (2008) suggests that $\ln S < -5$ is "strong" tension, $-5 < \ln S < -2.5$ is "moderate" tension, and $\ln S > -2.5$ indicates the data sets are in agreement.

We determine $\ln S$ using the ANESTHETIC software (W. Handley 2019), which produces an ensemble of realizations used to estimate sample variance. Results are quoted using the mean of the ensemble, with the error bars reflecting the standard deviation.

[100] Suspiciousness, S, is related to the Bayes ratio R and Bayesian information I and is defined as $\ln S = \ln R - \ln I$.

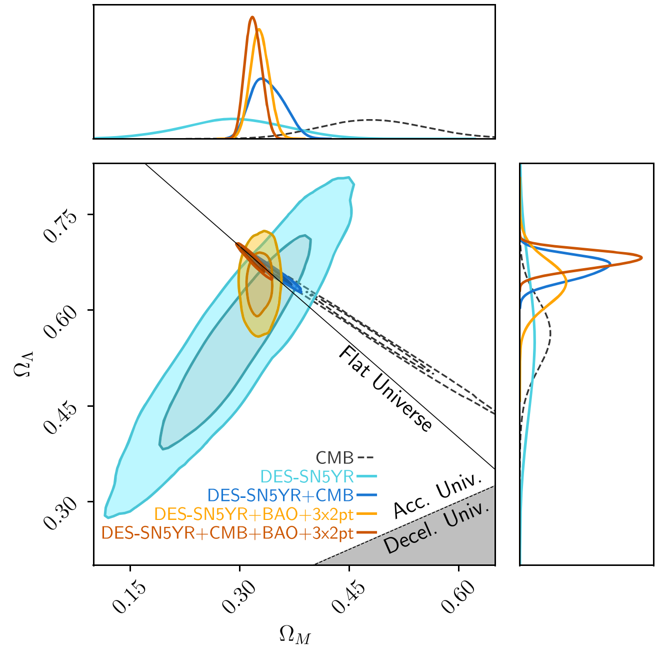

Figure 6. Constraints for the ΛCDM model (nonzero curvature allowed) from the DES-SN5YR data set only (cyan), DES-SN5YR combined with BAO $+3 \times 2$pt (orange), DES-SN5YR combined with CMB measurements (blue), and all these combined (red). For comparison, we also present cosmological constraints from Planck Collaboration (2020) only (black dashed).

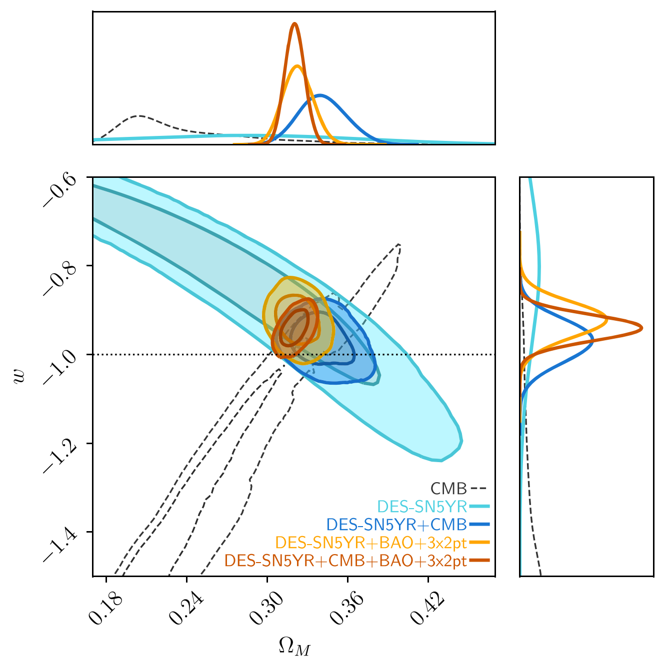

Figure 7. Same as Figure 6 but for the flat wCDM model. The horizontal dotted line marks the equation-of-state values for a cosmological constant, i.e., $w = -1$.

In Figure 9, we plot the suspiciousness values for the DES-SN5YR data versus Planck 2020 and versus BAO+3×2pt data. We find no indication of tension using any of the four models investigated in this Letter.

4.3. Model Selection

Finally, we use Bayesian evidence to test whether the extra parameters in the more complex models we test are warranted,

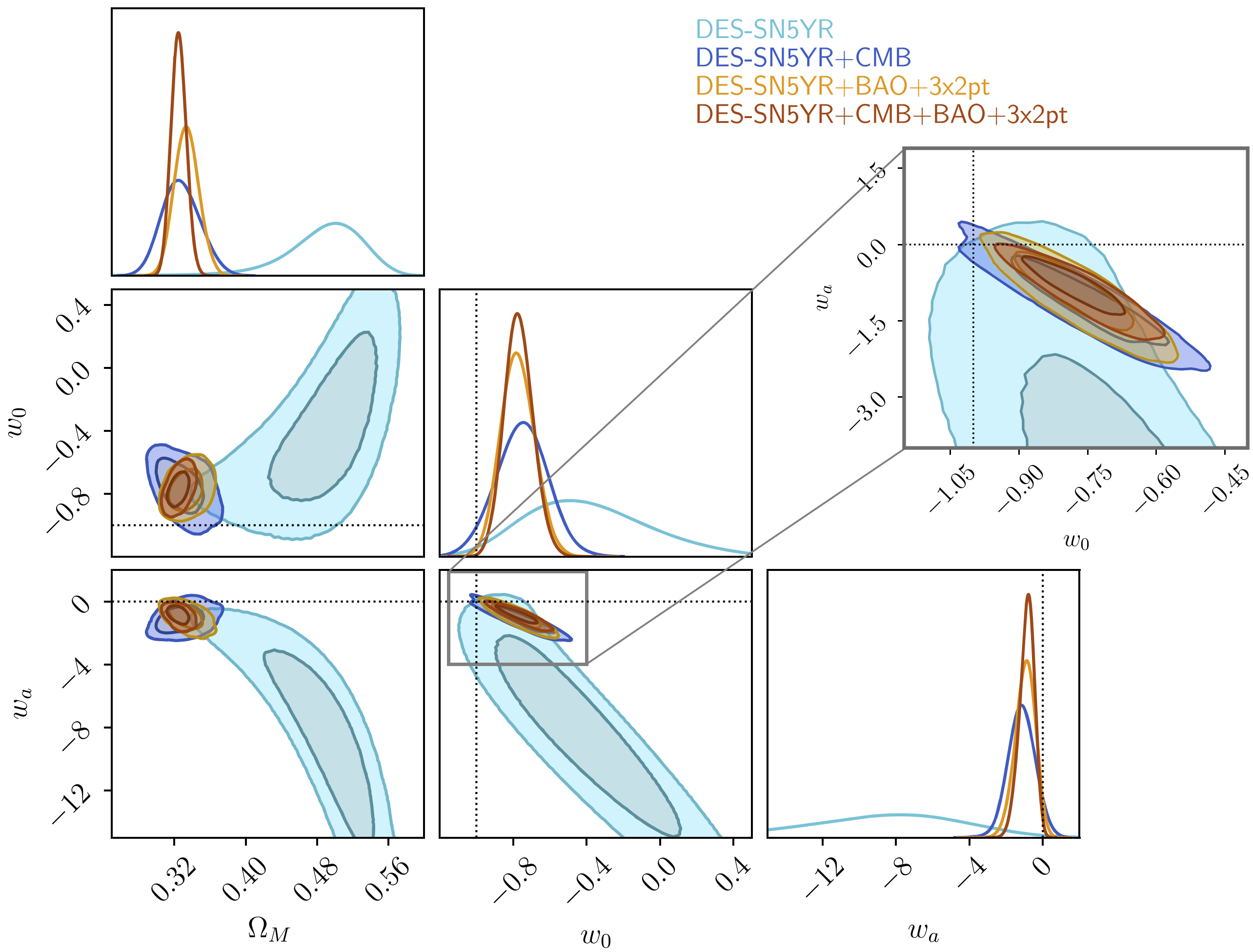

Figure 8. Same as Figure 6 but for the flat w_0w_aCDM model. The dashed crosshairs mark the equation-of-state values for a cosmological constant, i.e., (w_0, w_a) = (−1, 0). The residuals between the DES-SN5YR best-fit flat w_0w_aCDM with respect to the flat *w*CDM model are presented in Figure 4.

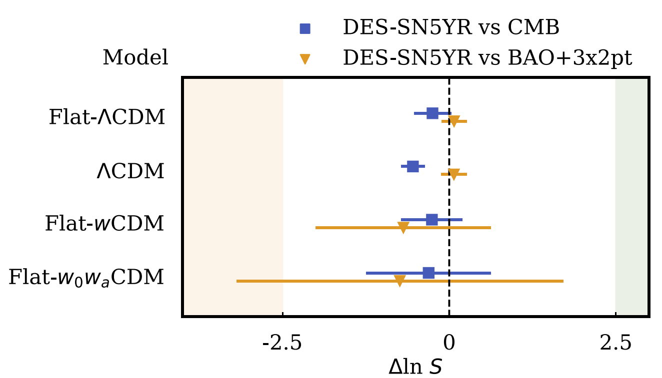

Figure 9. Measurements of suspiciousness (Δ ln(*S*)) between the DES-SN5YR and Planck 2020 data sets for the four models constrained in this Letter. Further left indicates higher tension, where the shaded regions reflect "moderate" (yellow) evidence of tension according to R. Trotta (2008). The values and uncertainties represent the mean and standard deviation of realizations estimating sample variance using the ANESTHETIC software.

given the data. In Figure 10, we present the difference in the logarithm of the Bayesian evidence, Δ(lnBE), relative to flat ΛCDM for the four different models tested in this analysis and the three combinations of data sets used in Figure 10.

To evaluate the strength of the evidence when comparing flat ΛCDM with more complex models, we again use Jeffreys's scale. This empirical scale suggests that Δ(ln*BE*) > 2.5 (and < −2.5) is moderate evidence against (in support of) the more complex model, whereas Δ(lnBE) > 5 (and < −5) is strong evidence against (in support of) the more complex model (for a review of model selection in cosmology, see R. Trotta 2008). We note that none of the data sets considered in this analysis strongly favor cosmological models beyond flat ΛCDM. The priors that we choose for model comparison are $w \in$ (–1.5, –0.5), $w_a \in$ (–10, 10), and $\Omega_K \in$ (–0.5, 0.5). We consider these priors (which determine the penalty for more complex models) to be reasonable in terms of general considerations, such as avoiding universes that are younger than generally accepted stellar ages (see Section 5.1.3). Although our chains have been run on uninformative priors, the Bayesian evidence from those chains may be adjusted for these harmonized priors as described in Appendix C.

5. Discussion

5.1. The Big Questions

5.1.1. Is the Expansion of the Universe Accelerating?

Twenty-five years ago, A. G. Riess et al. (1998) found 99.5%–99.9% (2.8σ–3.9σ) evidence for an accelerating Universe by considering the deceleration parameter $q \equiv (a\ddot{a})\dot{a}^{-2}$ and integrating over the likelihood that $q_0 < 0$. Importantly, they noted that since q_0 is measured at the present day but the

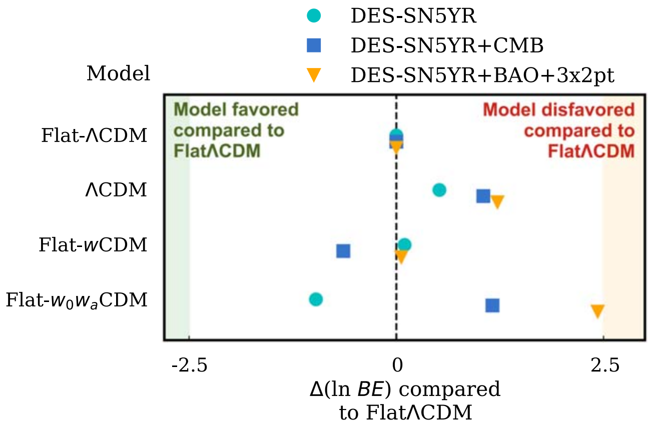

Figure 10. Bayesian evidence difference relative to flat ΛCDM (Δ(lnBE)). We present the results for the four different models tested in this analysis and the three combinations of data sets used (DES only in cyan, DES+Planck in blue, DES+BAO+3 × 2pt in orange). An increase (decrease) in Δ(lnBE) indicates that a model is disfavored (favored) compared to flat ΛCDM.

data span a wide range of redshifts, q_0 can only be measured within the context of a model, either cosmographic or physically motivated. They used the ΛCDM model, in which $q_0 = \Omega_M/2 - \Omega_\Lambda$.

Doing the same with DES-SN5YR data gives 99.99998% confidence (5.2σ) that $q_0 < 0$ in ΛCDM, or a 2×10^{-7} chance that the expansion of the Universe is not accelerating. As noted in Section 4.1.3, our confidence is even higher that the Universe *was* accelerating at $z \sim 0.2$. When we further assume flatness, the confidence in an accelerating Universe is overwhelming (no measurable likelihood for a decelerating Universe), and we find $q_0 = -0.530^{+0.018}_{-0.017}$. For more fits of q_0 using a cosmographic approach, see R. Camilleri et al. (2024).

5.1.2. Is Dark Energy a Cosmological Constant?

As seen in Section 4.1, a cosmological constant is a good fit to our data but not the best fit. Our best-fit equation-of-state parameter is slightly (more than 1σ) higher than the cosmological constant value of $w = -1$ (both for SNe alone and in combination with Planck or BAO+3 × 2pt). Our result agrees with the recent result from the UNION3 compilation analyzed with the UNITY framework (D. Rubin et al. 2023; which appeared while this Letter was under internal review). The Pantheon+ result (D. Brout et al. 2022a) is within 1σ of $w = -1$ but also on the high side ($w = -0.90 \pm 0.14$).

Furthermore, our analysis slightly prefers a time-varying dark energy equation-of-state parameter when we fit for $w(a)$ such that the equation-of-state parameter increases with time (again for all data combinations), known as a "thawing" model. Model selection, however, is inconclusive.

The constraints on time-varying w are enabled by the wide redshift range of the DES-SN5YR sample. Our analysis as described in M. Vincenzi et al. (2024) gives us confidence that systematic uncertainties in these data are below the level of our statistical precision. Nevertheless, it is important to recognize that (a) the low-z sample is the one for which we have the least systematic control, and (b) the very high-redshift SNe are the ones for which bias corrections are large (>0.1 mag) and more uncertain (e.g., accurate estimation of spectroscopic redshift efficiency is more challenging as we go to higher redshifts) and for which the uncertainties on the rest-frame UV part of the SN Ia SED have more impact on SN distance estimations (see also D. Brout et al. 2022a).

To test whether our fits are dominated by any particular redshift range, we ran cosmological fits (a) removing low-z data (i.e., DES SNe alone) and (b) removing high-z data (i.e., removing ∼80 SNe at $z > 0.85$, for which we use only two bands; see Figure 2). Most of the cosmological results obtained with the subsamples are consistent with the results found for the full sample. However, we found that removing the low-z sample shifts the contours in the flat wCDM slightly down, which would make the combined fits more consistent with $w = -1$. The flat w_0w_aCDM results are stable to subsample selection. See Appendix C for details.

We showed in M. Vincenzi et al. (2024) that systematic uncertainties are subdominant to the statistical uncertainties in our sample. Nevertheless, in the future, a new low-redshift sample (see Section 5.3) would help alleviate any remaining doubt about calibration and systematics in the existing low-z sample, and an even higher-redshift SN survey would help alleviate any modeling concerns by minimizing selection effects even at $z \sim 1$.

5.1.3. How Old Is the Universe?

One of the issues that the discovery of dark energy solved is the age of the Universe (t_0) problem—globular cluster age estimates, in combination with high estimates of H_0, were inconsistent with models that were not accelerating (D. A. VandenBerg et al. 1996; R. G. Gratton et al. 1997; B. Chaboyer et al. 1998).

Our results, which favor a dark energy equation-of-state parameter slightly higher than $w = -1$, would imply that the age is slightly *younger* than the age found in a Universe where dark energy is a cosmological constant (for the same values of H_0 and present dark energy density).

To calculate the Universe's age, one needs a value of H_0 in addition to the best-fit cosmological model. Since we do not constrain H_0 in this analysis, we present our measurement of the combination H_0t_0. In other words, we give t_0 in units of the Hubble time, $t_H \equiv 1/H_0$.[101] Our best-fit DES-SN5YR result in the flat ΛCDM would have an age of $(0.921 \pm 0.013)t_H$. This is ∼3% younger than Planck ($t_{\rm age}^{\rm Planck} = (0.950 \pm 0.007)t_H$), corresponding to an age difference of approximately −0.4 Gyr. Our best-fit flat w_0w_aCDM model gives an age of $(0.86 \pm 0.02)t_H$, about 9% younger than the flat ΛCDM Planck result, corresponding to an age difference of approximately −1.3 Gyr. Such a young age is unlikely given the age of the oldest globular clusters (D. Valcin et al. 2020; A. Cimatti & M. Moresco 2023; J. M. Ying et al. 2023). In the future, this information could be used as a prior to limit the feasible range of time-varying dark energy.

5.1.4. Does Our Best Fit Resolve the Hubble Tension?

As pointed out in Planck Collaboration (2020, their Section 5.4), the only basic extensions to the base flat ΛCDM model that resolve the H_0 tension are those in which the dark energy equation of state is allowed to vary away from $w = -1$. In the wCDM model, a phantom equation-of-state parameter of $w \sim -1.5$ would help resolve the tension (E. Di Valentino et al. 2021, their Section 5.1), and it is clear from Figure 7 that

[101] If $H_0 = 68$ km s^{-1} Mpc^{-1}, $t_H(68) = 14.38$ Gyr. If $H_0 = 73$ km s^{-1} Mpc^{-1}, $t_H(73) = 13.40$ Gyr.

CMB alone actually prefers $w < -1$. In this model, Planck alone does not constrain H_0 very tightly, and they refrain from quoting a value (see Table 5 of Planck Collaboration 2020), but lower w correlates with higher H_0. However, the DES-SN5YR data show a slight tendency for $w > -1$, essentially ruling out this solution within wCDM.

5.2. Comparison with DES-SN3YR and Pantheon+

It is informative to compare the results of the previous DES-SN3YR analysis (Dark Energy Survey Collaboration 2019; D. Brout et al. 2019a) with the results of the DES-SN5YR analysis presented in this work. The DES-SN3YR analysis included 207 *spectroscopically confirmed* SNe Ia from DES and 127 low-redshift SNe from Harvard-Smithsonian Center for Astrophysics (CfA) and CSP samples (see also Figure 3). A fraction of those events is in common between both analyses (55 from low-z external samples and 146 DES SNe).[102]

However, the DES-SN3YR analysis differs from the analysis presented here in many aspects. The SN Ia intrinsic scatter modeling has been significantly improved (from "G10" and a constant $\sigma_{\rm int}$ floor to the more sophisticated modeling of intrinsic scatter introduced by D. Brout & D. Scolnic 2021; B. Popovic et al. 2023), the BBC software has been updated (from BBC "5D" and a binned approach to BBC "4D" and an unbinned approach), the $x_1 - M_\star$ correlations have been incorporated into simulations (following the work by M. Smith et al. 2020b; B. Popovic et al. 2021), and the light-curve fitting model has been updated from the SALT2 model to the SALT3 model (see G. Taylor et al. 2023 for a comparison between SALT2 and SALT3 using the DES-SN3YR sample). Finally, the DES-SN3YR analysis did not require machine learning classification and the implementation of the BEAMS approach because it is a sample of spectroscopically selected SNe Ia. We compare the final SN distances in Figure 11 and find consistent results (differences in binned distances are on average 0.02 mag, even in the redshift ranges where contamination is expected to be high). The cosmological results from DES-SN3YR and DES-SN5YR are consistent within uncertainties (when assuming flat ΛCDM, $\Omega_{\rm M}$ are 0.331 ± 0.038 and 0.352 ± 0.017 for DES-SN3YR and DES-SN5YR, respectively, while when assuming flat wCDM and including CMB priors, w are -0.978 ± 0.059 and $-0.955^{+0.032}_{-0.037}$).

The other main data set we can compare to is Pantheon+, which contains a significant amount of independent data (all the high-z data). The DES sample is on average of much higher redshift than the Pantheon+ sample (see Figure 3), with over a quarter of the DES-SN5YR sample being at high enough redshift ($z \gtrsim 0.64$) to probe the likely *decelerating*[103] period of the Universe (compared to 6% in Pantheon+). We show a comparison of the contours in Figure 12. We find very similar constraining power between Pantheon+ and DES-SN5YR, and the DES-SN5YR value of w is within 1σ of Pantheon+ (D. Brout et al. 2022a). These analyses are not fully independent, as a fraction of the low-z sample is shared. However, all of the high-z data set is independent, and DES is a photometric sample, while Pantheon + is fully spectroscopic. The constraints on w are similar between DES and Pantheon+, as DES high-z has better precision per SN than Pantheon+ and has significantly higher statistical power at $z > 0.4$ (see Figure 3), but Pantheon+ used 2× more low-redshift SNe (which we do not include in order to be able to better control systematic uncertainties).

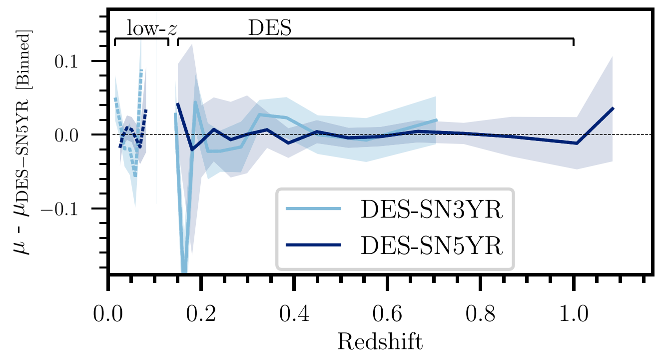

Figure 11. Comparison between Hubble residuals for the DES-SN3YR and DES-SN5YR analyses with respect to the best-fit flat wCDM for the DES-SN5YR analysis. Hubble residuals are binned in redshift, and we present the weighted mean and standard deviation of the mean in each redshift bin. The redshift range covered by the low-z sample is highlighted and shown with thick dotted lines. The two DES samples are consistent with each other. Note that the DES-SN3YR analysis only includes spectroscopically confirmed SNe, whereas the DES sample in the DES-SN5YR analysis consists entirely of photometrically identified SNe Ia and extends to higher z.

5.3. DES and Next-generation SN Samples

This analysis has shown that moving from a spectroscopically confirmed sample as done in Dark Energy Survey Collaboration (2019) to a photometric sample can increase the sample size of well-measured SNe significantly (from 207 DES SNe Ia in DES-SN3YR to >1600 in DES-5YR), consistent with an analysis of Pan-STARRS SNe in D. O. Jones et al. (2018). This improvement arises because photometric classification alleviates the bottleneck of limited spectroscopic resources. The improvement will increase for future surveys as more candidates are discovered, but the available time for spectroscopy does not increase commensurately. Importantly, the work of M. Vincenzi et al. (2024) shows that systematic uncertainties due to photometric classification are not limiting. Instead, the "conventional" systematics of calibration and modeling the intrinsic scatter remain the most significant challenges.

There is potential for a further increase of the statistical power of the DES sample if one moves to using SNe in which a host galaxy spectroscopic redshift was not acquired and instead relies on photometric redshifts of the SNe and the galaxy. This path was explored by R. Chen et al. (2022) for a subset of DES SNe, namely, ones that occur in redMaGiC galaxies, and has been explored as well for the SuperNova Legacy Survey (V. Ruhlmann-Kleider et al. 2022) and the Vera C. Rubin Observatory Legacy Survey of Space and Time (LSST) in A. Mitra et al. (2023). These analyses show that the use of photo-zs does not introduce systematic uncertainties to a scale similar to the statistical uncertainties. This potential is highlighted by the ≈2400 SNe Ia identified without host galaxy spectroscopic redshift in DES that could be used for this type of analysis (A. Möller & the DES Collaboration 2024, in preparation).

The DES SN survey was supported by the 6 yr OzDES survey on the Anglo-Australian Telescope (described in

[102] Not all events included in the DES-SN3YR analysis are included in the DES-SN5YR analysis, and vice versa. This is due to the two analyses implementing different sample cuts. For example, the $z > 0.025$ cut and the requirement for a host galaxy redshift in DES-SN5YR exclude, respectively, 44 and 29 low-z SNe that were in the DES-SN3YR sample. DES-SN5YR also uses a new SALT model (which affects the SALT-based cuts) and is restricted to SNe that pass selection cuts across all systematic tests (see Table 4 in M. Vincenzi et al. 2024).

[103] The redshift at which the Universe began accelerating in ΛCDM is $z_{\rm acc} = (2\Omega_\Lambda/\Omega_{\rm M})^{1/3} - 1$.

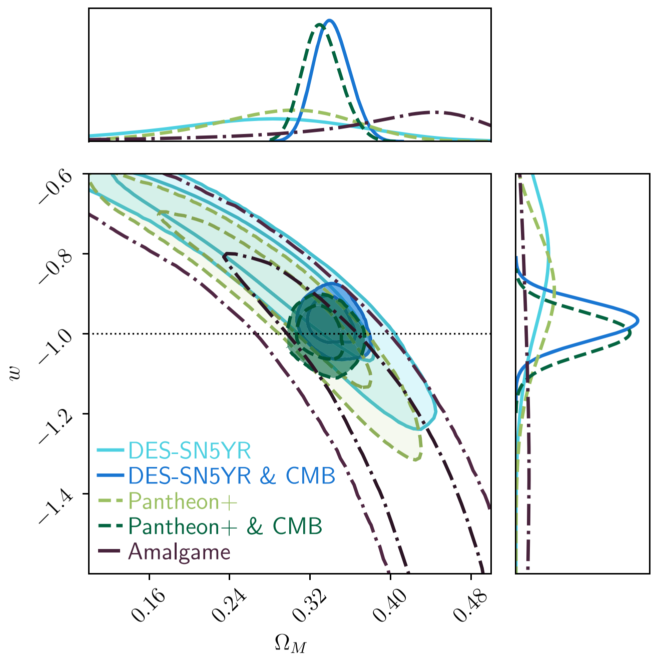

Figure 12. Constraints in flat wCDM from the DES-SN5YR sample, the Pantheon+ sample (with and without CMB priors), and the Amalgame sample. The constraining power of the DES-SN5YR and Pantheon+ samples is comparable and consistent, despite Pantheon+ being a spectroscopic SN Ia sample combining 17 different surveys. The "Amalgame" sample includes the SDSS and PS1 photometric SN samples (>1700 intermediate-redshift and high-redshift SNe); however, it does not include a low-z anchoring sample (hence the larger contours). DES-SN5YR and Pantheon+ are also combined with CMB constraints (for both, we use the Planck lite Python implementation presented by H. Prince & J. Dunkley 2019). The horizontal dotted line marks the equation-of-state values for a cosmological constant.

C. Lidman et al. 2020), which took multifiber observations of host galaxies to acquire redshifts of host galaxies of SNe. The total investment of this program was 100 nights, and for roughly 75% of the targeted host galaxies, a spectroscopic redshift has been secured. This program was fortuitous, as the cameras for OzDES and DECam have nearly identical fields of view. Enormous resources would be needed to reproduce this joint program for LSST, which will find millions of SNe across 18,000 deg^2 (Ivezić et al. 2019; B. O. Sánchez et al. 2022; compared to the 27 deg^2 of DES SNe). Surveys such as 4MOST will follow up tens of thousands of these (E. Swann et al. 2019), but the full wealth of transient information may benefit from an entirely photometric approach.

As statistical precision continues to improve thanks to the increased number of SNe, a main theme for systematic analysis is second-order relations between different systematics. Typically, systematics are treated independently when building the covariance matrix. We have implemented a method to account for calibration systematics along with light-curve model systematics together, but this is currently the only joint exercise. This type of work will grow in importance. For example, while photometric classification does not directly cause a large increase in the error budget, it hinders the ability to constrain the intrinsic scatter model preferred by the data. Potentially, if LSST and other surveys such as those enabled by the Nancy Grace Roman Space Telescope have enough SNe (B. M. Rose et al. 2021), the data set can enable a forward modeling approach such as the approximate Bayesian computation method introduced in E. Jennings et al. (2016) and worked on in P. Armstrong et al. (2024, in preparation), which could vary all systematics, nuisance, and cosmological parameters at the same time to compare against the data.

Furthermore, as discussed in Section 5.1.2, modeling of the low-z sample remains a source of systematic uncertainty. This sample comes from a multitude of surveys, even though we have removed many of the older inhomogeneous sources compared to analyses like Pantheon+. In the near future, we expect additions from the Zwicky Transient Facility (M. Smith 2024, in preparation), Young Supernova Experiment (D. O. Jones et al. 2021; P. D. Aleo et al. 2023), and Dark Energy Bedrock All-sky Supernova Survey (DEBASS; PI: Brout) to improve low-z constraints of the SN Hubble diagram, given their improved calibration and better-understood selection function.[104] DEBASS will be particularly fruitful as it is a low-redshift sample taken with DECam, so a single instrument and calibration catalog will be used for the full sample of DEBASS+DES, similar to the single-instrument PS1 sample in D. O. Jones et al. (2019). Using simulations, we estimate that quadrupling the size of our low-z sample (from ∼200 to ∼800 SNe expected from this next generation of low-z SN surveys) could enable a reduction of uncertainties on w by ∼30% (for a flat wCDM model using SN data alone).

Lastly, we note that while LSST and Roman may help improve a number of these issues, the first data release is still >3 yr away. We encourage work with the DES SN sample as presented here, combined with other samples. B. Popovic et al. (2024) recently showed the ability to combine separate photometric samples (PS1 and SDSS) into the Amalgame sample (also shown in Figure 12), and a similar analysis can be done by combining DES with these. It is reasonable to expect that with new low-redshift samples and a combination of high-redshift photometric samples, a sample with >5000 likely SNe Ia can be compiled in the very near future.

6. Conclusions

The DES SN survey stands as a groundbreaking milestone in SN cosmology. With a single survey, we effectively tripled the number of observed SNe Ia at $z > 0.2$ and quintupled the number beyond $z > 0.5$. Here we present the unblinded cosmological results, and in companion papers, we make public the calibrated light curves and Hubble diagram from the full sample of DES SNe Ia (B. O. Sánchez 2024; M. Vincenzi et al. 2024).

After combining the 1635 DES SNe (of which 1499 have a probability >0.5 of being a SN Ia) with 194 existing low-z SNe Ia, we present final cosmological results for four variants on ΛCDM cosmology, as summarized in Table 2.

The standard flat ΛCDM cosmological model is a good fit to our data. When fitting DES-SN5YR alone and allowing for a time-varying dark energy, we do see a slight preference for a dark energy equation of state that becomes greater (closer to 0) with time ($w_a < 0$), but this is only at the $\sim 2\sigma$ level, and Bayesian evidence ratios do not strongly prefer the flat $w_0 w_a$CDM cosmology.

We compare cosmological results from each of our models to results from the CMB analysis of Planck Collaboration (2020). There are some differences in the best-fit values, but in each case, we find consistency to within 2σ and a suspiciousness statistic that indicates agreement among the data sets.

[104] These upcoming low-z surveys are magnitude-limited rather than targeted; therefore, they provide SN samples with a well-defined selection function.

Critically, the DES-SN5YR analysis shown here demonstrates that contamination due to SN classification and host galaxy matching is not a limiting systematic for SN cosmology; this opens the path for a new era of cosmological measurements using SN samples that are not limited by live spectroscopic follow-up of SNe. Instead, our analysis shows the SN community that there are other factors that will be crucial for the success of future SN experiments: a high-quality low-redshift sample, a robust UV and near-IR extension of light-curve fitting models, excellent control of selection effects across the entire redshift range, and improvement in our understanding of SN Ia intrinsic scatter properties and the role played by interstellar dust.

Future work will conclude the DES by combining these SN results with the other three pillars of DES cosmology, namely, BAOs, galaxy clustering, and weak lensing.

Acknowledgments

We acknowledge the following former collaborators, who have contributed directly to this work: Ricard Casas, Pete Challis, Michael Childress, Ricardo Covarrubias, Chris D'Andrea, Alex Filippenko, David Finley, John Fisher, Francisco Förster, Daniel Goldstein, Santiago González-Gaitán, Ravi Gupta, Mario Hamuy, Steve Kuhlmann, James Lasker, Marisa March, John Marriner, Eric Morganson, Jennifer Mosher, Elizabeth Swann, Rollin Thomas, and Rachel Wolf.

T.M.D., A.C., R.C., and S.H. acknowledge the support of an Australian Research Council Australian Laureate Fellowship (FL180100168) funded by the Australian Government, and A.M. is supported by the ARC Discovery Early Career Researcher Award (DECRA) project No. DE230100055. M.S., H.Q., and J.L. are supported by DOE grant DE-FOA-0002424 and NSF grant AST-2108094. R.K. is supported by DOE grant DE-SC0009924. M.V. was partly supported by NASA through the NASA Hubble Fellowship grant HST-HF2-51546.001-A awarded by the Space Telescope Science Institute, which is operated by the Association of Universities for Research in Astronomy, Inc., under NASA contract NAS5-26555. L.K. thanks the UKRI Future Leaders Fellowship for support through the grant MR/T01881X/1. L.G. acknowledges financial support from the Spanish Ministerio de Ciencia e Innovación (MCIN), the Agencia Estatal de Investigación (AEI) 10.13039/501100011033, and the European Social Fund (ESF) "Investing in your future" under the 2019 Ramón y Cajal program RYC2019-027683-I and the PID2020-115253GA-I00 HOSTFLOWS project, from Centro Superior de Investigaciones Científicas (CSIC) under the PIE project 20215AT016, and the program Unidad de Excelencia María de Maeztu CEX2020-001058-M, and from the Departament de Recerca i Universitats de la Generalitat de Catalunya through the 2021-SGR-01270 grant. R.J.F. and D.S. were supported in part by NASA grant 14-WPS14-0048. The UCSC team is supported in part by NASA grants NNG16PJ34G and NNG17PX03C issued through the Roman Science Investigation Teams Program; NSF grants AST-1518052 and AST-1815935; NASA through grant No. AR-14296 from the Space Telescope Science Institute, which is operated by AURA, Inc., under NASA contract NAS 5-26555; the Gordon and Betty Moore Foundation; the Heising-Simons Foundation; and fellowships from the Alfred P. Sloan Foundation and the David and Lucile Packard Foundation to R.J.F. We acknowledge the University of Chicago's Research Computing Center for their support of this work.

Funding for the DES Projects has been provided by the U.S. Department of Energy, the U.S. National Science Foundation, the Ministry of Science and Education of Spain, the Science and Technology Facilities Council of the United Kingdom, the Higher Education Funding Council for England, the National Center for Supercomputing Applications at the University of Illinois at Urbana-Champaign, the Kavli Institute of Cosmological Physics at the University of Chicago, the Center for Cosmology and Astro-Particle Physics at the Ohio State University, the Mitchell Institute for Fundamental Physics and Astronomy at Texas A&M University, Financiadora de Estudos e Projetos, Fundação Carlos Chagas Filho de Amparo à Pesquisa do Estado do Rio de Janeiro, Conselho Nacional de Desenvolvimento Científico e Tecnológico and the Ministério da Ciência, Tecnologia e Inovação, the Deutsche Forschungsgemeinschaft, and the Collaborating Institutions in the Dark Energy Survey.

The Collaborating Institutions are Argonne National Laboratory, the University of California at Santa Cruz, the University of Cambridge, Centro de Investigaciones Energéticas, Medioambientales y Tecnológicas-Madrid, the University of Chicago, University College London, the DES-Brazil Consortium, the University of Edinburgh, the Eidgenössische Technische Hochschule (ETH) Zürich, Fermi National Accelerator Laboratory, the University of Illinois at Urbana-Champaign, the Institut de Ciències de l'Espai (IEEC/CSIC), the Institut de Física d'Altes Energies, Lawrence Berkeley National Laboratory, the Ludwig-Maximilians Universität München and the associated Excellence Cluster Universe, the University of Michigan, NSF's NOIRLab, the University of Nottingham, The Ohio State University, the University of Pennsylvania, the University of Portsmouth, SLAC National Accelerator Laboratory, Stanford University, the University of Sussex, Texas A&M University, and the OzDES Membership Consortium.

Based in part on observations at Cerro Tololo Inter-American Observatory at NSF's NOIRLab (NOIRLab Prop. ID 2012B-0001; PI: J. Frieman), which is managed by the Association of Universities for Research in Astronomy (AURA) under a cooperative agreement with the National Science Foundation. Based in part on data acquired at the Anglo-Australian Telescope. We acknowledge the traditional custodians of the land on which the AAT stands, the Gamilaraay people, and pay our respects to elders past and present. Parts of this research were supported by the Australian Research Council through project Nos. CE110001020, FL180100168, and DE230100055. Based in part on observations obtained at the international Gemini Observatory, a program of NSF's NOIRLab, which is managed by the Association of Universities for Research in Astronomy (AURA) under a cooperative agreement with the National Science Foundation on behalf of the Gemini Observatory partnership: the National Science Foundation (United States), National Research Council (Canada), Agencia Nacional de Investigación y Desarrollo (Chile), Ministerio de Ciencia, Tecnología e Innovación (Argentina), Ministério da Ciência, Tecnologia, Inovações e Comunicações (Brazil), and Korea Astronomy and Space Science Institute (Republic of Korea). This includes data from programs GN-2015B-Q-10, GN-2016B-LP-10, GN-2017B-LP-10, GS-2013B-Q-45, GS-2015B-Q-7, GS-2016B-LP-10, GS-2016B-Q-41, and GS-2017B-LP-10 (PI: Foley). Some of the data presented herein were obtained at Keck Observatory, which is a private 501(c)3 nonprofit organization operated as a scientific partnership among the California Institute of Technology, the University of California, and the National Aeronautics and Space Administration (PIs: Foley, Kirshner, and Nugent). The Observatory was made possible by the generous financial support of the W. M. Keck Foundation. This Letter includes results based on data gathered with the 6.5 m Magellan Telescopes located at Las Campanas Observatory, Chile (PI: Foley), and the Southern African Large Telescope (SALT; PIs: M. Smith & E. Kasai). The authors wish to recognize and acknowledge the very significant cultural role and reverence that the summit of Maunakea has always had within the Native Hawaiian community. We are most fortunate to have the opportunity to conduct observations from this mountain.

The DES data management system is supported by the National Science Foundation under grant Nos. AST-1138766 and AST-1536171. The DES participants from Spanish institutions are partially supported by MICINN under grants ESP2017-89838, PGC2018-094773, PGC2018-102021, SEV-2016-0588, SEV-2016-0597, and MDM-2015-0509, some of which include ERDF funds from the European Union. IFAE is partially funded by the CERCA program of the Generalitat de Catalunya. Research leading to these results has received funding from the European Research Council under the European Union's Seventh Framework Program (FP7/2007-2013) including ERC grant agreements 240672, 291329, and 306478. We acknowledge support from the Brazilian Instituto Nacional de Ciência e Tecnologia (INCT) do e-Universo (CNPq grant 465376/2014-2).

This research used resources of the National Energy Research Scientific Computing Center (NERSC), a U.S. Department of Energy Office of Science User Facility located at Lawrence Berkeley National Laboratory, operated under contract No. DE-AC02-05CH11231 using NERSC award HEP-ERCAP0023923. This manuscript has been authored by Fermi Research Alliance, LLC, under contract No. DE-AC02-07CH11359 with the U.S. Department of Energy, Office of Science, Office of High Energy Physics.

Facilities: Blanco, AAT, Gemini:Gillett (GMOS-N), Gemini:South (GMOS-S), Keck:I (LRIS), Keck:II (DEIMOS), Magellan:Baade (IMACS), Magellan:Clay (LDSS3, MagE), SALT.

Software: `numpy` (C. R. Harris et al. 2020), `astropy` (Astropy Collaboration 2013, 2018), `matplotlib` (J. D. Hunter 2007), `pandas` (Pandas development team 2020), `scipy` (P. Virtanen et al. 2020), `SNANA` (R. Kessler et al. 2009), `Pippin` (S. Hinton & D. Brout 2020), `ChainConsumer` (S. Hinton 2016), `SExtractor` (E. Bertin & S. Arnouts 1996), `MINUIT` (F. James & M. Roos 1975), SuperNNova (A. Möller & T. de Boissiere 2020), SCONE (H. Qu et al. 2021).

Appendix A
Data Release and How to Use the DES-SN5YR Data

Here we explain where to find the data and software necessary to reproduce our analysis. Many of the codes we use are already public (detailed below). The primary repository for our key data products is on Zenodo via DOI:10.5281/zenodo.12720778. We also mirror the key data and post code and tutorials on Github.[105]

The DES-SN5YR analysis was run using the PIPPIN pipeline framework (S. Hinton & D. Brout 2020)[106] that orchestrated SNANA codes for simulations, light-curve fitting, BBC, and covariance matrix computation (`SNANA`; R. Kessler et al. 2009)[107] and also integrated photometric classification from A. Möller & T. de Boissiere (2020)[108] and H. Qu et al. (2021).[109] Additional analysis codes that run outside the main pipeline include Scene Model Photometry (D. Brout et al. 2019b), fit to measure the SN population of stretch and color (B. Popovic et al. 2023)[110]; SALT3 training (W. D. Kenworthy et al. 2021)[111]; and CosmoSIS to fit for cosmological parameters (J. Zuntz et al. 2015).[112]

On Zenodo and Github, we release the PIPPIN input files necessary to (i) generate and fit all the simulations used in the analysis (both the large "biasCor" simulations to calculate bias corrections and the DES-SN5YR-like simulated samples to validate the analysis) and (ii) reproduce the full cosmological analysis, from light-curve fitting to photometric classification, distance estimates, and cosmological fitting. Auxiliary files are also available within the SNANA library[113] (R. Kessler & D. Brout 2020).

The various (intermediate and final) *outputs* of our analysis pipeline are also provided. This includes (i) light-curve fitted parameters, (ii) light-curve classification results, (iii) the final Hubble diagram and associated uncertainties covariance matrices, and (iv) the cosmology chains.

Appendix B
Priors

Table 3 lists the prior ranges for our MCMC chains. The priors related to external data sets align with the priors in the original papers. We adapted the prior ranges to enclose the majority of the high-likelihood region as appropriate for each data set and model combination. Data-set-specific priors are listed in the footnote to the table.

Bayesian evidence calculations depend on the choice of prior; larger prior ranges used on the same data and likelihoods lead to lower evidences, sometimes referred to as the *complex model penalty*. Therefore, in model comparison using evidence calculations, we took care to choose consistent prior ranges that do not unduly inflate this penalty. Bayes's theorem states

$$p(M|D) = \frac{p(D|M)p(M)}{p(D)} \propto p(D|M), \tag{B1}$$

where D is the data and M is the model, and the proportionality to the Bayesian evidence $p(D|M)$ follows from assuming no prior preference for any model. Writing the model parameters

[105] https://github.com/des-science/DES-SN5YR

[106] https://github.com/dessn/Pippin
[107] https://github.com/RickKessler/SNANA
[108] https://github.com/supernnova/SuperNNova
[109] https://github.com/helenqu/scone
[110] https://github.com/djbrout/dustdriver
[111] https://github.com/djones1040/SALTShaker
[112] https://github.com/joezuntz/cosmosis
[113] https://zenodo.org/records/4015325

Table 3
Priors[a]

Parameter	Prior	
Cosmology—baseline		
h	Flat	(0.55, 0.91)
$\Omega_{\rm m}$	Flat	(0.1, 0.9)
10^9 A_s	Flat	(0.5, 5.0)
$n_{\rm s}$	Flat	(0.87, 1.07)
$\Omega_{\rm b}$	Flat	(0.03, 0.07)
τ	Gaussian	(0.067, 0.023)
Ω_ν	Flat	(0.06, 0.6)
Lens Galaxy Bias		
$b_i(i \in [1, 4])$	Flat	(0.8, 3.0)
Lens Magnification		
C_1^1	Fixed	0.42
C_1^2	Fixed	0.30
C_1^3	Fixed	1.76
C_1^4	Fixed	1.94
Lens photo-z		
$\Delta z_1^1 \times 10^2$	Gaussian	(−0.9, 0.7)
$\Delta z_1^2 \times 10^2$	Gaussian	(−3.5, 1.1)
$\Delta z_1^3 \times 10^2$	Gaussian	(−0.5, 0.6)
$\Delta z_1^4 \times 10^2$	Gaussian	(−0.7, 0.6)
$\sigma_{2,1}^1$	Gaussian	(0.98, 0.06)
$\sigma_{z,1}^{2,1}$	Gaussian	(1.31, 0.09)
$\sigma_{z,1}^{31}$	Gaussian	(0.87, 0.05)
$\sigma_{\varepsilon,1}^4$	Gaussian	(0.92, 0.05)
Intrinsic Alignment		
$a_i(i \in [1, 2])$	Flat	(−5, 5)
$\alpha_i(i \in [1, 2])$	Flat	(−5, 5)
$b_{\rm TA}$	Flat	(0, 2)
z_0	Fixed	0.62
Source photo-z		
$\Delta z_s^1 \times 10^2$	Gaussian	(0.0, 1.8)
$\Delta z_{\rm s}^2 \times 10^2$	Gaussian	(0.0, 1.5)
$\Delta z_8^3 \times 10^2$	Gaussian	(0.0, 1.1)
$\Delta z_8^4 \times 10^2$	Gaussian	(0.0, 1.7)
Shear Calibration		
$m^1 \times 10^2$	Gaussian	(−0.6, 0.9)
$m^2 \times 10^2$	Gaussian	(−2.0, 0.8)
$m^3 \times 10^2$	Gaussian	(−2.4, 0.8)
$m^4 \times 10^2$	Gaussian	(−3.7, 0.8)

Model	Parameter	Prior	
Extended Models			
ΛCDM	Ω_K	Flat	(−0.5, 0.5)
Flat wCDM	w	Flat	(−2, 0)
Flat w_0w_aCDM	w_0	Flat	(−10, 5)
	w_a	Flat	(−20, 10)

Note.
[a] We also used some specific variations of the above baseline priors. For the ΛCDM model using the DES-SN5YR only, $\Omega_K \in (-1.2, 2)$; using DES-SN5YR + SDSS BAO and DES Y3 3 × 2pt, $\Omega_K \in (-0.8, 0.8)$; and using DES-SN5YR + Planck 2020 + SDSS BAO and DES Y3 3 × 2pt, $\Omega_K \in (-0.4, 0.4)$. For the flat wCDM model using DES-SN5YR + Planck 2020, $\Omega_{\rm m} \in (0.1, 1)$, and finally, for the flat w_0w_aCDM model using DES-SN5YR + SDSS BAO and DES Y3 3 × 2pt, $w_0 \in -(2, 0)$.

as $\vec{\theta}$, we can then write

$$p(D|M) = \int p(D, \vec{\theta}|M) d^N\theta$$
$$= \int p(D|\vec{\theta}, M) p(\vec{\theta}) d^N\theta = p(\vec{\theta}) \int p(D|\vec{\theta}, M) d^N\theta, \quad \text{(B2)}$$

where the last step assumes a constant prior for each of the N parameters θ_i of model M that fully encompasses the support of the likelihood function (this is true to a very good approximation for the models that are tested here). Making explicit the dependence of the Bayesian evidence on the model prior by writing $p(D|M) = \mathrm{BE}(\vec{\theta})$, the evidence may then be adjusted for a change in prior volume without recomputing the chains as follows:

$$\ln \mathrm{BE}(\vec{\theta}_2) = \ln \mathrm{BE}(\vec{\theta}_1) + \ln p(\vec{\theta}_1) - \ln p(\vec{\theta}_2)\ , \quad \text{(B3)}$$

where using $(\theta_{i,\rm min}, \theta_{i,\rm max})$ for the prior range for each parameter,

$$p(\vec{\theta}) = \prod_{i=1}^{N} \frac{1}{\theta_{i,\rm max} - \theta_{i,\rm min}}. \quad \text{(B4)}$$

Appendix C
Tests on Subsets of Our Data

The large redshift range of the DES-SN5YR sample provides a strong lever arm on the measurement of any time variation of dark energy. We therefore check for potential peculiarities at the extremes of our redshift range that are driving the fit toward non-cosmological-constant values.

In Figure 13 and Table 4, we show the change to the flat ΛCDM, flat wCDM, and flat w_0w_aCDM fits using DES SNe alone (no low-z external samples) and when using the full DES-SN5YR sample but excluding the highest-redshift SNe ($z > 0.85$, the 5% highest-redshift events in our DES SN sample). We show, for example, that in flat ΛCDM, excluding the low-z sample lowers the best-fit value to $\Omega_{\rm M}^{\text{no low}-z} = 0.330 \pm 0.024$ ($\Delta\Omega_{\rm M} = -0.022$), which is in closer agreement with the CMB value of $\Omega_{\rm M}^{\rm Planck} = 0.317 \pm 0.008$. Similarly, excluding high-redshift SNe lowers the best-fit value to $\Omega_{\rm M}^{\text{no high}-z} = 0.342 \pm 0.017$ ($\Delta\Omega_{\rm M} = -0.010$). However, it is important to quantify the significance of the observed shifts.

The cosmological contours using the full DES-SN5YR sample, the DES-SN5YR sample without low-z, and the DES-SN5YR sample without high-z cannot be *directly compared* as if they were three independent measurements (the three data sets used have large overlaps). Therefore, in order to examine the significance of the observed shifts, we generate 100 independent realizations of the DES-SN5YR Hubble diagram applying the Cholesky decomposition to the full DES-SN5YR data vector of 1829 SNe and the associated 1829 × 1829 statistical and systematic covariance matrix. For each independent realization, we fit the cosmological parameters with and without the low-z and high-z samples and estimate the *standard deviation* (σ) of the estimated $\Delta\Omega_{\rm M}$ (or Δw and/or Δw_0 and Δw_a when fitting for flat wCDM and flat w_0w_aCDM). Using

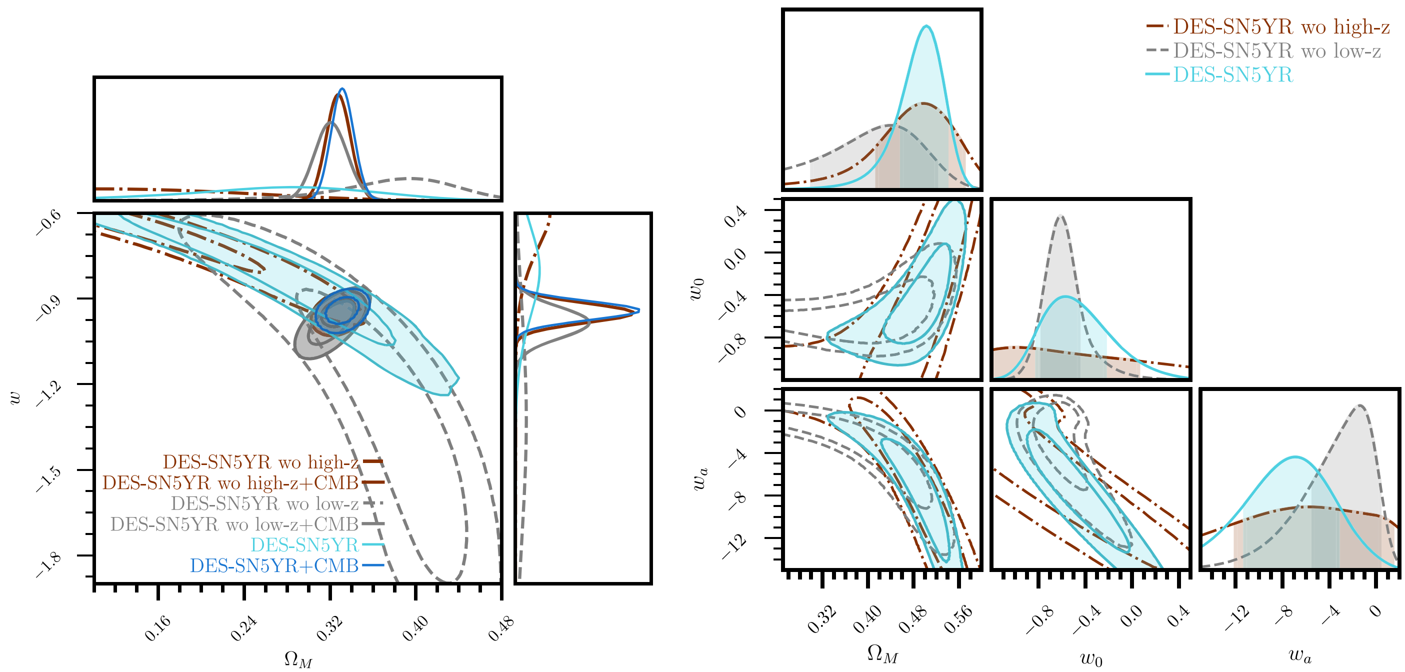

Figure 13. Constraints for the full DES-SN5YR data set (cyan), when excluding low-z SNe ($z < 0.1$; gray dashed line), and when excluding high-z SNe ($z > 0.85$; brown dotted–dashed line). In flat wCDM (left), the contours shift primarily along the degeneracy line (and in opposite directions for the low-z and high-z cuts) but also slightly perpendicular to the degeneracy direction. In combination with the CMB prior, this pushes the result closer to $w = -1$ in the no-low-z case. The flat w_0w_aCDM model (right) best fit sees no significant shifts with subsample selection.

Table 4
Results Using DES Data Alone (Excluding Low-z below $z < 0.1$) and DES-SN5YR without High-z SNe ($z < 0.85$)

	Ω_M [$\Delta\Omega_M$]	w_0 [Δw_0]	w_a	Shift Significance
DES SNe without Low-z				
Flat ΛCDM	0.330 ± 0.024 [-0.022]	⋯	⋯	1.1σ in Ω_M
Flat wCDM	0.373 ± 0.058	-1.34 ± 0.32 [0.54]	⋯	2.3σ in w
Flat wCDM + Planck-like prior	0.321 ± 0.013	-0.985 ± 0.048 [0.043]†	⋯	1.1σ in w
Flat w_0w_aCDM	0.460 ± 0.100	-0.58 ± 0.74 [0.22]	-6.9 ± 6.0 [-1.9]	$<1\sigma$ in w_0 and w_a
DES SNe without High-z				
Flat ΛCDM	0.342 ± 0.017 [-0.010]	⋯	⋯	2.1σ in Ω_M
Flat wCDM	0.139 ± 0.088	-0.66 ± 0.11 [-0.14]	⋯	-2.2σ in w
Flat wCDM + Planck-like prior	0.328 ± 0.010	-0.951 ± 0.030 [0.009]†	⋯	1.9σ in w
Flat w_0w_aCDM	0.363 ± 0.123	-0.58 ± 0.18 [0.22]	-3.7 ± 3.2 [-5.1]	$<1\sigma$ in w_0 and w_a

Note. Shift significance: the significance of shifts in either Ω_M (when fitting for the flat ΛCDM model) or w (when testing flat wCDM) is estimated from 100 simulations.

[a] Using the CMB-prior approximation described in the text, we obtain a value of $w = -0.942 \pm 0.030$, instead of the value of $w = -0.955^{+0.032}_{-0.037}$ presented in Table 2. For consistency, Δw in this table are calculated with respect to the w value calculated using the CMB-prior approximation.

this approach, we measure a $\sigma(\Delta\Omega_M)$ of 0.02 and 0.005 when fitting for flat ΛCDM and excluding low-z and high-z SNe, respectively, and we conclude that the $\Delta\Omega_M$ observed on the real data are significant at 1.1σ and 2.1σ, respectively.

In flat wCDM, excluding low-z gives a best-fit $w = -1.34 \pm 0.32$ ($\Delta w = 0.54$), and excluding high-z gives a best-fit $w = -0.66 \pm 0.11$ ($\Delta w = -0.14$). Using our 100 realizations with systematics, we estimate that the significance of the shifts is 2.3σ and -2.2σ, respectively.

We perform the same test incorporating a CMB-like prior. Estimating the best-fit flat wCDM from our SN subsamples combined with the full CMB likelihood from Planck Collaboration (2020) is computationally expensive and practically unfeasible for data and 100 simulations. For this reason, we use an approximation of a CMB-like prior that uses the R parameter (defined, e.g., in E. Komatsu et al. 2009, see their Equation (69)) from Planck Collaboration (2020). This CMB-prior approximation is incorporated in the fast minimization cosmological fitting program `wfit`, available in SNANA. When combining SNe and the approximated CMB prior and fitting for flat wCDM, we find that the shifts observed in w are not statistically significant (less than 2σ).

We make similar tests for the flat w_0w_aCDM model. The main results are consistent for the different redshift cuts, with the central value varying less than the flat wCDM case despite (or because of) the extra flexibility of flat w_0w_aCDM.

If there are no statistical fluctuations, the observed shifts in w when removing either low- or high-z SNe would be expected if the flat *w*CDM model is inadequate and cannot simultaneously fit the both low- and high-redshift range in our data; but it is also what you expect if there is some kind of systematic error in the low-z or high-z data. Future independent data sets (both SNe and other measures of expansion such as BAOs) are essential to determine which is the better explanation. The seemingly large values of some of the shifts in cosmological parameters are due to the strong degeneracy in the w–Ω_M plane, as seen in Figure 13. Once combined with external data, such as a CMB prior, it is more evident that the shift perpendicular to the degeneracy direction is small (e.g., third line of Table 4).

ORCID iDs

DES Collaboration: T. M. C. Abbott https://orcid.org/0000-0003-1587-3931
O. Alves https://orcid.org/0000-0002-7394-9466
J. Annis https://orcid.org/0000-0002-0609-3987
P. Armstrong https://orcid.org/0000-0003-1997-3649
K. Bechtol https://orcid.org/0000-0001-8156-0429
P. H. Bernardinelli https://orcid.org/0000-0003-0743-9422
G. M. Bernstein https://orcid.org/0000-0002-8613-8259
E. Bertin https://orcid.org/0000-0002-3602-3664
S. Bocquet https://orcid.org/0000-0002-4900-805X
D. Brooks https://orcid.org/0000-0002-8458-5047
D. Brout https://orcid.org/0000-0001-5201-8374
D. L. Burke https://orcid.org/0000-0003-1866-1950
A. Carnero Rosell https://orcid.org/0000-0003-3044-5150
D. Carollo https://orcid.org/0000-0003-4710-132X
A. Carr https://orcid.org/0000-0003-4074-5659
J. Carretero https://orcid.org/0000-0002-3130-0204
F. J. Castander https://orcid.org/0000-0001-7316-4573
C. Chang https://orcid.org/0000-0002-7887-0896
R. Chen https://orcid.org/0000-0003-3917-0966
C. Conselice https://orcid.org/0000-0003-1949-7638
L. N. da Costa https://orcid.org/0000-0002-7731-277X
M. Crocce https://orcid.org/0000-0002-9745-6228
T. M. Davis https://orcid.org/0000-0002-4213-8783
S. Desai https://orcid.org/0000-0002-0466-3288
H. T. Diehl https://orcid.org/0000-0002-8357-7467
C. Doux https://orcid.org/0000-0003-4480-0096
A. Drlica-Wagner https://orcid.org/0000-0001-8251-933X
J. Elvin-Poole https://orcid.org/0000-0001-5148-9203
I. Ferrero https://orcid.org/0000-0002-1295-1132
R. J. Foley https://orcid.org/0000-0002-2445-5275
P. Fosalba https://orcid.org/0000-0002-1510-5214
D. Friedel https://orcid.org/0000-0002-3632-7668
C. Frohmaier https://orcid.org/0000-0001-9553-4723
J. García-Bellido https://orcid.org/0000-0002-9370-8360
E. Gaztanaga https://orcid.org/0000-0001-9632-0815
K. Glazebrook https://orcid.org/0000-0002-3254-9044
O. Graur https://orcid.org/0000-0002-4391-6137
R. A. Gruendl https://orcid.org/0000-0002-4588-6517
S. R. Hinton https://orcid.org/0000-0003-2071-9349
D. L. Hollowood https://orcid.org/0000-0002-9369-4157
D. Huterer https://orcid.org/0000-0001-6558-0112
D. J. James https://orcid.org/0000-0001-5160-4486
S. Kent https://orcid.org/0000-0003-4207-7420
R. Kessler https://orcid.org/0000-0003-3221-0419
A. G. Kim https://orcid.org/0000-0001-6315-8743
E. Kovacs https://orcid.org/0000-0002-2545-1989
K. Kuehn https://orcid.org/0000-0003-0120-0808
J. Lee https://orcid.org/0000-0001-6633-9793
G. F. Lewis https://orcid.org/0000-0003-3081-9319
T. S. Li https://orcid.org/0000-0002-9110-6163
C. Lidman https://orcid.org/0000-0003-1731-0497
H. Lin https://orcid.org/0000-0002-7825-3206
P. Martini https://orcid.org/0000-0002-0194-4017
J. Mena-Fernández https://orcid.org/0000-0001-9497-7266
F. Menanteau https://orcid.org/0000-0002-1372-2534
R. Miquel https://orcid.org/0000-0002-6610-4836
J. Mould https://orcid.org/0000-0003-3820-1740
E. Neilsen https://orcid.org/0000-0002-7357-0317
P. Nugent https://orcid.org/0000-0002-3389-0586
R. L. C. Ogando https://orcid.org/0000-0003-2120-1154
Y.-C. Pan https://orcid.org/0000-0001-8415-6720
A. Pieres https://orcid.org/0000-0001-9186-6042
H. Qu https://orcid.org/0000-0003-1899-9791
A. K. Romer https://orcid.org/0000-0002-9328-879X
A. Roodman https://orcid.org/0000-0001-5326-3486
M. Sako https://orcid.org/0000-0003-2764-7093
E. Sanchez https://orcid.org/0000-0002-9646-8198
J. Allyn. Smith https://orcid.org/0000-0002-6261-4601
M. Smith https://orcid.org/000-0002-3321-1432
M. Soares-Santos https://orcid.org/0000-0001-6082-8529
E. Suchyta https://orcid.org/0000-0002-7047-9358
M. Sullivan https://orcid.org/0000-0001-9053-4820
N. Suntzeff https://orcid.org/0000-0002-8102-181
M. E. C. Swanson https://orcid.org/0000-0002-1488-8552
G. Tarle https://orcid.org/0000-0003-1704-078
D. Thomas https://orcid.org/0000-0002-6325-5671
C. To https://orcid.org/0000-0001-7836-2261
B. E. Tucker https://orcid.org/0000-0002-4283-5159
D. L. Tucker https://orcid.org/0000-0001-7211-5729
S. A. Uddin https://orcid.org/0000-0002-9413-4186
A. R. Walker https://orcid.org/0000-0002-7123-8943
N. Weaverdyck https://orcid.org/0000-0001-9382-5199
R. H. Wechsler https://orcid.org/0000-0003-2229-011X
W. Wester https://orcid.org/0000-0003-0072-6736

References

Alam, S., Ata, M., Bailey, S., et al. 2017, MNRAS, 470, 2617
Alam, S., Aubert, M., Avila, S., et al. 2021, PhRvD, 103, 083533
Alard, C., & Lupton, R. H. 1998, ApJ, 503, 325
Aleo, P. D., Malanchev, K., Sharief, S., et al. 2023, ApJS, 266, 9
Armstrong, P., Qu, H., Brout, D., et al. 2023, PASA, 40, e038
Astropy Collaboration 2013, A&A, 558, A33
Astropy Collaboration 2018, AJ, 156, 123
Bautista, J. E., Paviot, R., Vargas Magaña, M., et al. 2021, MNRAS, 500, 736
Bernstein, J. P., Kessler, R., Kuhlmann, S., et al. 2012, ApJ, 753, 152
Bertin, E., & Arnouts, S. 1996, A&AS, 117, 393
Betoule, M., Kessler, R., Guy, J., et al. 2014, A&A, 568, A22
Blanton, M. R., Bershady, M. A., Abolfathi, B., et al. 2017, AJ, 154, 28
Brout, D., Hinton, S. R., & Scolnic, D. 2021, ApJL, 912, L26
Brout, D., & Scolnic, D. 2021, ApJ, 909, 26
Brout, D., Scolnic, D., Kessler, R., et al. 2019a, ApJ, 874, 150
Brout, D., Sako, M., Scolnic, D., et al. 2019b, ApJ, 874, 106
Brout, D., Scolnic, D., Popovic, B., et al. 2022a, ApJ, 938, 110
Brout, D., Taylor, G., Scolnic, D., et al. 2022b, ApJ, 938, 111
Burke, D. L., Rykoff, E. S., Allam, S., et al. 2018, AJ, 155, 41
Camilleri, R., Davis, T. M., Vincenzi, M., et al. 2024, MNRAS, 533, 2615
Chaboyer, B., Demarque, P., Kernan, P. J., & Krauss, L. M. 1998, ApJ, 494, 96
Chen, R., Scolnic, D., Rozo, E., et al. 2022, ApJ, 938, 62
Chen, R., Scolnic, D., Rozo, E., et al. 2022, ApJ, 938, 62
Chevallier, M., & Polarski, D. 2001, IJMPD, 10, 213
Childress, M. J., Lidman, C., Davis, T. M., et al. 2017, MNRAS, 472, 273
Cimatti, A., & Moresco, M. 2023, ApJ, 953, 149
Conley, A., Guy, J., Sullivan, M., et al. 2011, ApJS, 192, 1
Dark Energy Survey Collaboration 2016, MNRAS, 460, 1270
Dark Energy Survey Collaboration 2019, ApJL, 872, L30

Dark Energy Survey Collaboration 2022, PhRvD, 105, 023520
Dark Energy Survey Collaboration 2023, PhRvD, 107, 083504
Dawson, K. S., Kneib, J.-P., Percival, W. J., et al. 2016, AJ, 151, 44
de Mattia, A., Ruhlmann-Kleider, V., Raichoor, A., et al. 2021, MNRAS, 501, 5616
Di Valentino, E., Mena, O., Pan, S., et al. 2021, CQGra, 38, 153001
Diehl, H. T., Neilsen, E., Gruendl, R., et al. 2016, Proc. SPIE, 9910, 99101D
Diehl, H. T., Neilsen, E., Gruendl, R. A., et al. 2018, Proc. SPIE, 10704, 107040D
Dixon, M., Lidman, C., Mould, J., et al. 2022, MNRAS, 517, 4291
du Mas des Bourboux, H., Rich, J., Font-Ribera, A., et al. 2020, ApJ, 901, 153
Duarte, J., González-Gaitán, S., Mourao, A., et al. 2023, A&A, 680, A56
Fioc, M., & Rocca-Volmerange, B. 1999, arXiv:astro-ph/9912179
Flaugher, B., Diehl, H. T., Honscheid, K., et al. 2015, AJ, 150, 150
Foley, R. J., Scolnic, D., Rest, A., et al. 2017, MNRAS, 475, 193
Foreman-Mackey, D., Hogg, D. W., Lang, D., & Goodman, J. 2013, PASP, 125, 306
Ganeshalingam, M., Li, W., & Filippenko, A. V. 2013, MNRAS, 433, 2240
Gilliland, R. L., Nugent, P. E., & Phillips, M. M. 1999, ApJ, 521, 30
Gratton, R. G., Pecci, F. F., Carretta, E., et al. 1997, ApJ, 491, 749
Gupta, R. R., Kuhlmann, S., Kovacs, E., et al. 2016, AJ, 152, 154
Handley, W. 2019, JOSS, 4, 1414
Handley, W., & Lemos, P. 2019, PhRvD, 100, 023512
Handley, W. J., Hobson, M. P., & Lasenby, A. N. 2015, MNRAS, 450, L61
Harris, C. R., Millman, K. J., van der Walt, S. J., et al. 2020, Natur, 585, 357
Hicken, M., Challis, P., Jha, S., et al. 2009, ApJ, 700, 331
Hicken, M., Challis, P., Kirshner, R. P., et al. 2012, ApJS, 200, 12
Hinton, S., & Brout, D. 2020, JOSS, 5, 2122
Hinton, S. 2016, JOSS, 1, 00045
Hlozek, R., Kunz, M., Bassett, B., et al. 2012, ApJ, 752, 79
Hou, J., Sánchez, A. G., Ross, A. J., et al. 2021, MNRAS, 500, 1201
Hunter, J. D. 2007, CSE, 9, 90
Ivezić, Ž., Kahn, S. M., Tyson, J. A., et al. 2019, ApJ, 873, 111
James, F., & Roos, M. 1975, CoPhC, 10, 343
Jennings, E., Wolf, R., & Sako, M. 2016, arXiv:1611.03087
Jones, D. O., Foley, R. J., Narayan, G., et al. 2021, ApJ, 908, 143
Jones, D. O., Scolnic, D. M., Foley, R. J., et al. 2019, ApJ, 881, 19
Jones, D. O., Scolnic, D. M., Riess, A. G., et al. 2018, ApJ, 857, 51
Kelsey, L., Sullivan, M., Wiseman, P., et al. 2023, MNRAS, 519, 3046
Kenworthy, W. D., Jones, D. O., Dai, M., et al. 2021, ApJ, 923, 265
Kessler, R., & Brout, D. 2020, SNDATA_ROOT for SNANA software, v4, Zenodo, doi:10.5281/zenodo.4015325
Kessler, R., Bernstein, J. P., Cinabro, D., et al. 2009, PASP, 121, 1028
Kessler, R., Brout, D., D'Andrea, C. B., et al. 2019a, MNRAS, 485, 1171
Kessler, R., Guy, J., Marriner, J., et al. 2013, ApJ, 764, 48
Kessler, R., Marriner, J., Childress, M., et al. 2015, AJ, 150, 172
Kessler, R., Narayan, G., Avelino, A., et al. 2019b, PASP, 131, 094501
Kessler, R., & Scolnic, D. 2017, ApJ, 836, 56
Kessler, R., Vincenzi, M., & Armstrong, P. 2023, ApJL, 952, L8
Komatsu, E., Dunkley, J., Nolta, M. R., et al. 2009, ApJS, 180, 330
Krisciunas, K., Contreras, C., Burns, C. R., et al. 2017, AJ, 154, 211
Kunz, M., Bassett, B. A., & Hlozek, R. A. 2007, PhRvD, 75, 103508
Kunz, M., Hlozek, R., Bassett, B. A., et al. 2012, in Astrostatistical Challenges for the New Astronomy, ed. J. M. Hilbe (New York: Springer), 63
Lahav, O., Calder, L., Mayers, J., & Frieman, J. 2020, The Dark Energy Survey (Singapore: World Scientific), https://www.worldscientific.com/doi/pdf/10.1142/q0247
Lasker, J., Kessler, R., Scolnic, D., et al. 2019, MNRAS, 485, 5329
Lee, J., Acevedo, M., Sako, M., et al. 2023, AJ, 165, 222
Lemos, P., Raveri, M., Campos, A., et al. 2021, MNRAS, 505, 6179
Lidman, C., Tucker, B. E., Davis, T. M., et al. 2020, MNRAS, 496, 19
Linder, E. V. 2003, PhRvL, 90, 091301
Marriner, J., Bernstein, J. P., Kessler, R., et al. 2011, ApJ, 740, 72
Meldorf, C., Palmese, A., Brout, D., et al. 2023, MNRAS, 518, 1985
Mitra, A., Kessler, R., More, S., Hlozek, R. & LSST Dark Energy Science Collaboration 2023, ApJ, 944, 212
Möller, A., & de Boissiere, T. 2020, MNRAS, 491, 4277
Möller, A., Smith, M., Sako, M., et al. 2022, MNRAS, 514, 5159
Pandas development team 2020, Zenodo: pandas-dev/pandas: Pandas, v2.2.2, Zenodo, doi:10.5281/zenodo.3509134
Perlmutter, S., Aldering, G., Goldhaber, G., et al. 1999, ApJ, 517, 565
Phillips, M. M., Lira, P., Suntzeff, N. B., et al. 1999, AJ, 118, 1766
Planck Collaboration 2020, A&A, 641, A6
Popovic, B., Brout, D., Kessler, R., & Scolnic, D. 2023, ApJ, 945, 84
Popovic, B., Brout, D., Kessler, R., Scolnic, D., & Lu, L. 2021, ApJ, 913, 49
Popovic, B., Scolnic, D., Vincenzi, M., et al. 2024, MNRAS, 529, 2100
Prince, H., & Dunkley, J. 2019, PhRvD, 100, 083502
Pskovskii, I. P. 1977, SvA, 21, 675
Qu, H., Sako, M., Möller, A., & Doux, C. 2021, AJ, 162, 67
Qu, H., Sako, M., Vincenzi, M., et al. 2024, ApJ, 964, 134
Riess, A. G., Filippenko, A. V., Challis, P., et al. 1998, AJ, 116, 1009
Riess, A. G., Nugent, P. E., Gilliland, R. L., et al. 2001, ApJ, 560, 49
Riess, A. G., Rodney, S. A., Scolnic, D. M., et al. 2018, ApJ, 853, 126
Riess, A. G., Strolger, L.-G., Tonry, J., et al. 2004, ApJ, 607, 665
Riess, A. G., Strolger, L.-G., Casertano, S., et al. 2007, ApJ, 659, 98
Rose, B. M., Baltay, C., Hounsell, R., et al. 2021, arXiv:2111.03081
Ross, A. J., Samushia, L., Howlett, C., et al. 2015, MNRAS, 449, 835
Rubin, D., Aldering, G., Betoule, M., et al. 2023, arXiv:2311.12098
Ruhlmann-Kleider, V., Lidman, C., & Möller, A. 2022, JCAP, 2022, 065
Rust, B. W. 1974, PhD thesis, Oak Ridge National Laboratory, Tennessee
Rykoff, E. S. 2023, Rykoff, Eli S. 2023. "The Dark Energy Survey Six–Year Calibration Star Catalog", FERMILAB–TM–2784-PPD-SCD, Fermi Technical Note, doi:10.2172/1973601
Sako, M., Bassett, B., Becker, A. C., et al. 2018, PASP, 130, 064002
Sánchez, B. O., Brout, D., Vincenzi, M., et al. 2024, arXiv:2406.05046
Sánchez, B. O., Kessler, R., Scolnic, D., et al. 2022, ApJ, 934, 96
Scolnic, D., Brout, D., Carr, A., et al. 2022, ApJ, 938, 113
Scolnic, D. M., Jones, D. O., Rest, A., et al. 2018, ApJ, 859, 101
Sevilla-Noarbe, I., Bechtol, K., Kind, M. C., et al. 2021, ApJS, 254, 24
Smith, M., D'Andrea, C. B., Sullivan, M., et al. 2020a, AJ, 160, 267
Smith, M., Sullivan, M., Wiseman, P., et al. 2020b, MNRAS, 494, 4426
Stevens, A. R. H., Bellstedt, S., Elahi, P. J., & Murphy, M. T. 2020, NatAs, 4, 843
Sullivan, M., Le Borgne, D., Pritchet, C. J., et al. 2006, ApJ, 648, 868
Sullivan, M., Guy, J., Conley, A., et al. 2011, ApJ, 737, 102
Suzuki, N., Rubin, D., Lidman, C., et al. 2012, ApJ, 746, 85
Swann, E., Sullivan, M., Carrick, J., et al. 2019, Msngr, 175, 58
Taylor, G., Jones, D. O., Popovic, B., et al. 2023, MNRAS, 520, 5209
The Dark Energy Survey Collaboration 2005, arXiv:astro-ph/0510346
Tripp, R. 1998, A&A, 331, 815
Trotta, R. 2008, ConPh, 49, 71
Valcin, D., Bernal, J. L., Jimenez, R., Verde, L., & Wandelt, B. D. 2020, JCAP, 2020, 002
VandenBerg, D. A., Bolte, M., & Stetson, P. B. 1996, ARA&A, 34, 461
Vincenzi, M., Sullivan, M., Firth, R. E., et al. 2019, MNRAS, 489, 5802
Vincenzi, M., Sullivan, M., Graur, O., et al. 2021, MNRAS, 505, 2819
Vincenzi, M., Sullivan, M., Möller, A., et al. 2023, MNRAS, 518, 1106
Vincenzi, M., Brout, D., Armstrong, P., et al. 2024, arXiv:2401.02945
Virtanen, P., Gommers, R., Oliphant, T. E., et al. 2020, NatMe, 17, 261
Wiseman, P., Smith, M., Childress, M., et al. 2020, MNRAS, 495, 4040
Wiseman, P., Sullivan, M., Smith, M., et al. 2021, MNRAS, 506, 3330
Wiseman, P., Vincenzi, M., Sullivan, M., et al. 2022, MNRAS, 515, 4587
Ying, J. M., Chaboyer, B., Boudreaux, E. M., et al. 2023, AJ, 166, 18
Yuan, F., Lidman, C., Davis, T. M., et al. 2015, MNRAS, 452, 3047
Zuntz, J., Paterno, M., Jennings, E., et al. 2015, A&C, 12, 45